This document was prepared in conjunction with work accomplished under Contract No. DE-AC09-76SR00001 with the U.S. Department of Energy.

DISCLAIMER

Key Words

L Lake
L Reactor
Cooling Lake Model

TECHNICAL DIVISION
SAVANNAH RIVER LABORATORY

DPST-84-496
Revision 1, 1/1/85

Distribution

S. Mirshak, Wilm, M-6600
R. M. Harbour, Wilm, M-6600
G. F. Merz, 703-A, A-239
C. P. Ross, 703-A
F. Beranek, 707-C
D. R. Muhlbaier, 707-C
J. T. Lowe, 773-A
T. V. Crawford, 773-A
J. D. Spencer, 773-A
M. R. Buckner, 773-A
A. L. Boni, 773-A
J. F. Proctor, 773-A
M. M. Anderson, 773-A
D. H. Stephenson, 773-A
A. J. Garrett, 786-1A
J. D. Menna, 773-23A
W. G. McMillan, 735-A
R. W. Benjamin, 773-A
D. W. Hayes, 773-11A
SRL Records (4)

M E M O R A N D U M

May 31, 1984

TO: M. R. BUCKNER

FROM: A. J. GARRETT, D. W. HAYES, W. G. McMILLAN

AJ Garrett

LAGRANGIAN AND CONTROL VOLUME MODELS FOR PREDICTION OF COOLING LAKE PERFORMANCE AT SRP

BASIS FOR REISSUE

This report is being reissued to make it a readily available supporting document for the work done by J. D. Menna (DPST-84-969) on operational control of L Reactor and the 1000 acre cooling lake now being constructed. The report also contains new material on model validation (see Figure 6).

CONTENTS

1. Abstract

Lagrangian and control volume cooling lake models are developed and tested with a 31 year meteorological data base and observations from the SRP Par Pond system. Turbulent transport of sensible and latent heat from the lake surface is described as well as solar and thermal radiative energy transfer. Primary results of the model validation are: long term mean monthly temperatures were predicted to within 1°C in the summer and to within 1 to 3°C in the winter. Temperatures are predicted as accurately in the warmer areas of Par Pond as in the colder parts. Root-Mean-Square-Errors (RMSE) associated with predictions of individual monthly means were about 1°C in the summer and 2°C in the winter. RMSE's associated with daily temperature predictions in the summer are about 1°C, with individual prediction errors as large as 3°C. The level of model skill demonstrated in the validation with the Par Pond data base indicates that the temperature distributions presented by Cooper (1984) are reliable.

Analysis of the Par Pond data base revealed that lake surface temperatures exceeding 32.2°C (90°F) are attained occasionally in the summer in areas where there is little or no heating from the P-Area Reactor. Regulations which seek to keep surface temperatures below 32.2°C should be structured to allow for these naturally occurring thermal excursions.

2. Introduction

The success of the proposed cooling lake for the SRP L-Area Reactor depends on the ability of the lake to cool heated water from the reactor sufficiently for a balanced biological system to exist in the lower half of the lake. The mathematical models described in this document and the companion document by Cooper (1984) were used to predict the cooling performance of the L-Area Reactor lake to be located in the Steel Creek basin. This document includes descriptions of methods used to calculate turbulent heat and radiative energy transfer, Lagrangian and control volume models, model validation methods, data bases, and model validation results. The companion document by Cooper describes the model used to predict horizontal temperature distributions within the proposed lake on a seasonal basis, and it presents those distributions.

3. Model Development

3.1 Lagrangian Model

All cooling lake models that are not entirely statistical must make use of the conservation equation for internal energy. Advective and turbulent exchange processes are dominant in cooling lakes, so molecular diffusion can be neglected. This simplification allows the rate of change of temperature of a fluid layer to be written as:

$$\rho_w c_{pw} \int_{-h}^{o} \frac{dT}{dt} dz = H_s + H_L + S + L_w \qquad (1)$$

where

ρ_w = density of water (1 gm cm^{-3})

c_{pw} = specific heat of water (1 cal gm^{-1} K^{-1})

T = temperature of water (K)

h = depth of fluid layer (m)

z = vertical coordinate

H_s = sensible heat flux to atmosphere (cal m^{-2} s^{-1})

H_L = latent heat flux to atmosphere (cal m^{-2} s^{-1})

S = net solar radiation flux (cal m^{-2} s^{-1})

L_w = net longwave (thermal) radiation flux (cal m^{-2} s^{-1})

The derivative in Eq. 1 is the substantial derivative, i.e.,

$$\frac{d}{dt} = \frac{\partial}{\partial t} + u \frac{\partial}{\partial x} + v \frac{\partial}{\partial y} + w \frac{\partial}{\partial z} \qquad (2)$$

where t, x, y, and z refer to time and the 3 space coordinates and u, v, and w are the corresponding velocity components.

Assuming that the fluid layer is well mixed down to h allows T in Eq. 1 to be replaced by the vertical average, $\bar{T}$. Integration and rearrangement of the equation gives:

$$\frac{d\bar{T}}{dt} = \frac{H_S + H_L + S + L_w}{h \ \rho_w \ c_{pw}} \qquad (3)$$

Methods for calculation of H_s, H_L, S, and L_w are given in Section 3.3. A method for estimating h (2.4 m in these calculations) will be described in a report to be issued in the near future.

3.2 Control Volume Model

Eq. (3) can be written as

$$\frac{\partial \bar{T}}{\partial t} = - u \frac{\partial \bar{T}}{\partial x} + F_T \tag{4}$$

where

$$F_T = \frac{H_S + H_L + S + L_w}{h \rho_w c_{pw}} \tag{5}$$

The expanded derivative (Eq. 2) was simplified by the assumption of no vertical transport ($w = 0$), except near the reactor outfall, as shown later. Also, it was assumed that mean transport is along the x axis, lateral turbulent diffusion (aided by buoyancy force) creates uniform temperatures perpendicular to the transport (x) axis, and diffusion along the transport axis is negligible.

Dropping the overbar on T and rewriting (4) in finite difference form (using upstream differencing) gives:

$$\frac{T_j^{i+1} - T_j^{i}}{\Delta t} = \frac{u_j \left(T_{j-1}^{i+1} - T_j^{i+1} \right)}{\Delta x} + F_{Tj}^{i} \tag{6}$$

where i superscripts refer to time and j subscripts refer to space. The transport velocity u can be defined by

$$u_j = \frac{Q_j D_v}{A_j} \tag{7}$$

where Q_j is the flow rate through the lake ($m^3\ s^{-1}$), D_v is the dilution factor ($D_v > 1$) which accounts for mixing at the reactor outfall, and A_j is the crossectional area of a lake sector represented by node j ($A_j = h\Delta y_j$). In the simplest version of the

model, all flow rates and crossectional areas are the same, so the j subscript can be dropped. Inserting Eq. 7 into Eq. 6 yields

$$\frac{Q\left(T_{j-1}^{i+1} - T_j^{i+1}\right)}{h\Delta x\Delta y} = \frac{Q\, D_v\left(T_{j-1}^{i+1} - T_j^{i+1}\right)}{h\, A_s} \qquad (8)$$

where A_s is the sector surface area, which is a quantity readily determined from topographic maps.

The final form of the equation is

$$\frac{T_j^{i+1} - T_j^{i}}{\Delta t} = \frac{Q\, D_v\left(T_{j-1}^{i+1} - T_j^{i+1}\right)}{h\, A_s} + F_{T_j}^{i} \qquad (9)$$

which is valid for all sectors downstream from the first one ($j = 2, 3, 4, \ldots N$). In the first sector, hot water from the reactor at a flow rate Q is mixed with subsurface water returning from the lower (dam) end of the lake. The amount of mixing is determined by the dilution factor D_v. For sector 1, the governing equation is:

$$\frac{\left(T_1^{i+1} - T_1^{i}\right)}{\Delta t} = \frac{Q\left(T_R - T_1^{i+1}\right)}{h\, A_s} + \frac{Q\left(D_v - 1\right)\left(T_N^{i} - T_1^{i+1}\right)}{h\, A_s} + F_{T_1}^{i} \qquad (10)$$

In Eq. 10, T_R is the reactor outfall temperature and T_N is the temperature at the dam. It is assumed that the water needed for dilution at the reactor outfall sinks near the dam and returns to the outfall sector as a reverse current underneath the hot surface layer. A schematic of the conceptual model that Eqs. 9 and 10 are based on is shown in Fig. 1. Eqs. 9 and 10 are essentially a control volume model, as shown in Fig. 1.

The model described above is similar but simpler than models described by Ryan and Harleman (1973), Jirka et al (1978) and Adams et al (1980). The primary simplification is the omission of longitudinal diffusion. This is not considered to be a problem for several reasons. First, model predictions of temperatures in Par Pond at the SRP are close to the observed temperatures (see Section 5). Second, the simple methods for estimating diffusion that are used in the Jirka and Adams models, such as Fischer's (1967) equation, are more appropriate for narrow streams than large cooling lakes. Wind stresses and the buoyancy force make diffusion of hot water in a cooling lake considerably more complex than indicated by Fischer's equation.

3.3 Calculation of D_v

The magnitude of the dilution factor D_v has significant effects on predicted temperature distributions. Empirical values of D_v can be determined from temperature measurements and a simple mass budget involving inflow (reactor outfall) temperature T_i, subsurface return flow temperature T_B, and the mixing zone temperature T_M:

$$T_M = P\ T_i + (1 - P)T_B \tag{11}$$

where P is the proportion ($0 \leq P \leq 1$) of reactor outfall water in the mixture. Solving for P:

$$P = \frac{T_M - T_B}{T_i - T_B} = \frac{1}{D_v} \tag{12}$$

The relationship between P and D_V follows from the definition of a dilution factor.

Temperature measurements on 4/2/84 and 4/6/84 in the canal just above Pond C, in the mixing zone, and at the bottom of Pond C generated the following values of P and D_V.

	P	D_V
4/2/84	0.79	1.27
4/6/84	0.86	1.16

Corresponding measurements at the lower end of Pond C, in the Bubble-Up (mixing zone) of Par Pond just down from Pond C, and the bottom of Par Pond generated the values given below.

	P	D_V
4/2/84	0.38	2.63
4/6/84	0.33	3.03

These values of D_V are comparable to those found by Neill and Babcock (1971), whose average over 13 trials was 2.3, with extremes of 1.0 and 4.5.

The large differences between D_V's at the entrances of Pond C and Par Pond were caused by the different inflow designs. In Pond C, water from the P Reactor canal spreads into a fan-shaped outfall as it enters a shallow (1 m) arm of the lake. The shallow arm inhibits mixing by reducing the amount of colder bottom water that comes into contact with the canal water near the outfall where velocities are large and turbulence is strong. The large temperature differential (15 to 20°C) plus the reduced velocities at the

mixing point keep the Froude number small. In contrast, water from Pond C enters Par Pond from a submerged pipe, which greatly enhances mixing.

3.4 Energy Flux Calculations

3.4.1 Solar Radiation

When global solar radiation measurements are not available, then the solar flux must be calculated. Latitude, cloud cover, and atmospheric water vapor content must be accounted for. The solar model described below was developed and tested by Garrett (1978), (1980), (1982).

Clear sky global solar radiation is calculated from

$$F = F_o \left(T_d \; T_{ws}^{w} \; T_{wa}^{w} \right)^{M} \cos \theta \qquad (13)$$

In Eq. 13, T_d, T_{ws}, and T_{wa} are transmission functions which parameterize the effects of dry air scattering, water vapor scattering, and water vapor absorption, respectively. The exponent w is total atmospheric water vapor content expressed as an equivalent water depth (cm), and M is a pressure-adjusted optical depth. The coefficient F_o is the solar flux above the troposphere, and Θ is the zenith angle.

The pressure-adjusted optical depth M is defined by

$$M = \frac{mp}{p_o} \qquad (14)$$

where m is the optical depth, p is atmospheric pressure at the location of interest and p_o is sea level pressure (1013.25 millibars). The optical depth is defined by

$$m = \sec \Theta \qquad (15)$$

for $\Theta < 70°$, and by

$$m = \frac{R \cos \Theta + \left(R^2 \cos^2 \Theta + 2RH + H^2\right)^{1/2}}{H} \qquad (16)$$

for $\Theta > 70°$.

In Eq. 17, R is the radius of the earth (6370 km) and H is an atmospheric scale height (10 km).

The transmission functions and F_o are defined by

$$T_d = 0.9 + 0.01\,(-0.1\,m^2 + 1.3\,m - 0.6) \qquad (17)$$

$$T_{ws} = 0.975 \qquad (18)$$

$$T_{wa} = 1 - 0.19685 \Big/ \left[1 + 1 \Big/ \left\{0.6992\,\left(w_m\right)^{1/2}\right\}\right] \qquad (19)$$

$$F_o = 0.98 S_o\,(\phi m/\phi)^2 \qquad (20)$$

In Eq. 20, S_o is the solar constant (1.94 cal cm^{-2} s^{-1}), 0.98 is a coefficient accounting for solar absorption by ozone in the stratosphere, ϕ_m is the mean earth to sun distance of 1.49×10^8 km, and ϕ is the actual distance, which is a function of the Julian day (J):

$$\phi = 149 - 2.6 \sin\,[\pi/2 - J\pi/182.5] \qquad (21)$$

When clouds are present, transmission functions must be used to deplete the solar flux. Cumulus and stratocumulus are usually the dominant depleters of solar radiation. Transmission functions for these cloud types are:

$$t_{cu} = 0.17 - 0.21\ Y \qquad 0 \leq Y \leq 0.2 \tag{22}$$

$$t_{st} = 0.28 - 0.16\ Y \tag{23}$$

$$t_{st} = 0.19 + 0.28\ Y \tag{24}$$

$$t_{cu} = -0.10 + 0.14\ Y \qquad 0.2 \leq Y \leq 1 \tag{25}$$

where $Y = \cos \Theta$, and t_{cu} and t_{st} are the transmission functions for cumulus and stratocumulus.

The net surface global radiation is

$$S = F\left(1 - A\right)\left(1 - \sigma_c + \sigma_c t\right) \tag{26}$$

where A is albedo of water, σ_c is the amount of cloud cover ($0 \leq \sigma_c \leq 1$), and t is the cloud transmission function. The albedo (A) is computed from relationships presented by Kondratyev (1969)

$$A = \frac{1}{2}\left[\frac{\sin^2 (i-r)}{\sin^2 (i+r)} + \frac{\tan^2 (i-r)\ \cos^2 (i+r)}{\sin^2 (i+r)}\right] \tag{27}$$

where r is the angle of refraction and i is the angle of incidence, which are related through n, the refractive index (n = 1.33).

$$\sin r = \frac{\sin i}{n} \tag{28}$$

3.4.2 Longwave Radiation

The net surface longwave radiative flux is calculated with a simplified transmission model that treats emission and absorption in combined spectral bands. The model was developed by Kondratyev (1969), and modified by Garrett (1977). Clouds are treated as blackbodies and emission and absorption above the tropopause is neglected. The general case of partly cloudy skies is treated. The flux contributed by a spectral group j is computed from

$$L_{wj} = 4\,\sigma\,\overline{T^3}\,(T_s - T_1) + p_j \sum_{i=1}^{I_c}\left[\frac{\phi i}{k_j}\left(e^{-k_j w_{i+1}} - e^{-k_j w_i}\right)\right]$$

$$+ (1-\sigma_c)\left\{p_j \sum_{i=I_{c+1}}^{I_T}\left[\frac{\phi i}{k_j}\left(e^{-k_j w_{i+1}} - e^{-k_j w_i}\right)\right]\right.$$

$$\left. + p_j\, e^{-k_j w_I}\, B(T_I)\right\} \qquad (29)$$

where

$$\phi_i = \frac{B\,(w_{i+1}) - B\,(w_i)}{w_{i+1} - w_i} \qquad (30)$$

and

$$L_w = \sum_{j=1}^{J} L_{wj} \qquad (31)$$

In Eq. 29,

σ = Stefan-Boltzmann constant

T_s = water surface temperature (K)

T_1 = surface layer air temperature (at 50 m)

$\overline{T^3} = (T_1^3 + T_s^3)/2$

p_j = weighting coefficient

k_j = absorption coefficient

w = atmospheric equivalent water depth (cm)

σ_c = cloud cover

B = blackbody flux (σT^4)

i = computational level

I_c = cloud level

I = tropopause level

The absorption and weighting coefficients in Eq. 29 are given below.

$p_1 = 0.25$ $\quad$ $p_2 = 0.11$

$k_1 = 0.166$ $\quad$ $k_2 = 0.8$

Garrett (1977) showed that the temperature and moisture structure of the middle and upper troposphere is not a critical factor in the calculation of L_w. So for all atmospheric layers above the lowest kilometer, the temperature is computed with

$$T(z) = T_a + \Gamma z \tag{32}$$

where T_a is the mean monthly surface layer temperature, and Γ is the standard atmospheric lapse rate (-6.5°C/km).

The equivalent liquid atmospheric water content is computed from

$$w(z) = w_T \left(1 - e^{-z/\ell} \right) \tag{33}$$

where w_T is the total tropospheric equivalent water depth and ℓ is a length scale computed from a large number of atmospheric soundings (ℓ = 2 km). The monthly values of w and T used in the computations are given below:

	J	F	M	A	M	J	J	A	S	O	N	D
T(°F)	47.6	49.3	54.9	63.2	71.6	78.9	80.7	80.2	75.3	65.2	54.1	47.2
w(cm)	2.0	2.0	2.5	2.5	2.5	3.0	3.0	3.0	2.5	2.5	2.5	2.0

The mean temperatures given above were taken from Climates of the States (NOAA, 1974) and cover the period from 1931 through 1960. The mean w values were derived from numerous atmospheric

soundings and include pressure corrections. The top of the computational domain was set at 15 km (top of the troposphere).

3.4.3 Turbulent Sensible and Latent Heat Fluxes

Several methods have been developed to calculate turbulent fluxes of sensible and latent heat from and to solid or liquid surfaces. Brutsaert (1981) reviews these methods and recommends flux profile-based methods. The general, efficient method developed by Louis (1979) was used in the model described in this report because it extends the flux-profile approach to include the free convection limit. Free convection is infrequent in the atmosphere, because some prevailing wind is almost always present. However, a strongly heated surface in the presence of weak winds will produce strong buoyancy-generated turbulence that approximates the free convection regime.

Louis' method makes use of a bulk Richardson number for the atmospheric surface layer.

$$B = \frac{gz\Delta\Theta}{\overline{\Theta}\, U^2} \qquad (34)$$

where g is gravitational acceleration (9.8 m s^{-2})

$\Delta\Theta$ = potential temperature difference across the surface layer ($\Theta_{50m} - \Theta$ water).

$\overline{\Theta}$ = mean potential temperature in surface layer

U = wind speed.

The fluxes can be written as

$$H_S = \frac{a^2 U \Delta\Theta F \rho_a C_p}{R} \tag{35}$$

$$H_L = \frac{a^2 U \Delta q F \rho_a L}{R} \tag{36}$$

where $R = 0.74$, ρ_a = air density, C_p = specific heat of air, L = latent heat of condensation, F = flux profile parameterization using B, Δq = specific humidity difference across the surface layer and

$$a^2 = k^2 / \left\{ \ln \left(z/z_o \right) \right\}^2 \tag{37}$$

where k = von Karman's constant (0.4)

z_o = roughness length over water (0.0002 m).

The flux profile parameterization F is defined by

$$F = 1 - \frac{bB}{1 + C|B|^{1/2}} \tag{38}$$

for $B < 0$, and

$$F = \frac{1}{\left(1 + \frac{bB}{2}\right)^2} \tag{39}$$

for $B > 0$. In Eqs. 38 and 39,

$b = 9.4$, and

$$C = 5.3 a^2 b \left(z/z_o\right)^{1/2} \tag{40}$$

3.5 Numerical Methods

Eqs. 9 and 10 could be solved directly, except for the non-linear flux terms involving T_j. An iterative predictor-corrector method is used instead, in which T_j^{i+1} is calculated and then

used in all flux terms for an improved estimate of T_j^{i+1}. Three iterations are sufficient, because convergence is rapid. Some numerical diffusion is generated by the numerical approximation to the advection terms, but it does not appear to be significant relative to the simplifying assumptions discussed earlier or to model performance (see Section 5). The numerical integration is performed with a 1 hour timestep, which is short compared to the maximum permissible timestep of about 5 hours (ΔX is 200 m or more, U is around 1 cm s^{-1}).

4. Sensitivity Analysis

Both models described in Section 3 are most sensitive to the evaporative heat loss equations (Section 3.4.3), because evaporation is the primary mechanism for heat loss from a cooling lake. The wind speed U enters directly into the evaporation calculation (Eq. 36) and indirectly via the bulk Richardson number (Eqs. 34, 38, and 39). The observed magnitude of U in these equations must be referenced to an appropriate height in the atmosphere. The meteorological data used in these model calculations included wind speeds measured at 6 meters (20 feet). Air flowing over a 1000 acre (4 km^2) cooling lake will develop an internal boundary layer at least 50 m thick. This estimate is based on the rough rule that a boundary layer developing downwind from a roughness discontinuity will have about a 0.1 slope. The proposed L Area cooling lake will be at least several hundred meters wide at all points, so 50 m is an appropriate reference level for the winds and temperatures ($z = 50$ m in Eqs. 34, 37, and 40).

If the 6 m Augusta meteorological data was not referenced to a higher elevation, then unrealistically large gradients of temperature and specific humidity would be maintained in the calculations. This would cause overestimates of the heat losses. Direct referencing of the temperatures and specific humidities to a 50 m height is possible because temperature and moisture gradients between 6 and 50 m over homogeneous terrain are small. For example, a 10°C/km lapse rate implies only a 0.44°C temperature decrease over that layer.

Wind speeds, however, do change significantly between 6 and 50 m. Irwin (1979) presents empirical power law coefficients that allow the change in U over a lower atmospheric layer to be computed as a function of stability. Irwin's data show that for mixed agricultural and forest land (z_o ~0.1 m) U increases by about 25% in unstable conditions (categories A, B and C) and by about a factor of two in stable conditions (category E). These corrections were applied to the computations by increasing U by 25% when the observed solar flux was greater than 40 cal m^{-2} s^{-1}, and by a factor of two when the solar flux was smaller.

Fig. 2 shows the result of running the control volume model (Section 3.2) with 31 years of hourly meteorological data from Augusta with (PROFILE) and without (PRED) the corrections to U described above. Monthly average results are shown in Fig. 2. The model sensitivity is about 1 to 2°C. The temperatures and specific humidities used in the computations for the PRED curve were

referenced to 50 m. If they also had been referenced to 6 m, much larger differences would have been generated.

The wind speed correction described above is a simplified solution to a complex problem. The internal boundary-layer over a cooling lake will deepen from the upwind to the downwind side of the lake; 50 m is an estimate of the average depth. The mean depth of the internal boundary layer will change with wind direction (parallel or perpendicular to the lake axis). The decrease in roughness over the lake will cause an acceleration of the winds, so the 25 to 100% increase in speed may occur below 50 m. Despite these uncertainties, the referencing to 50 m appears to be justified on physical and empirical grounds (see Section 5).

Another way to determine model sensitivity is to compare predictions from similar but independently developed models. Fig. 3 shows the NUS (Firstenburg and Fisher, 1980) and SRL control volume model predictions of the proposed L-Lake mean monthly surface temperatures with distance from the reactor outfall. The SRL model predicts cooler temperatures at the lower end of the lake, although the models are close to each other in their predictions of the temperature at the 50% point in the summer (32°C for NUS, 31.2°C for SRL). SRL predicts somewhat lower equilibrium temperatures than the NUS model and thus calls for more cooling at the lower end of the lake. The model predictions will be compared to temperature data from the SRP Par Pond in Section 5.

5. Statistical Methods and Model Verification

5.1 Overview of Methods

Validation of environmental models requires the use of several statistical tests of skill, because a given model may perform well according to one test, and poorly according to another. The three basic measures of skill are bias, dispersion, and correlation. An evaluation of bias shows whether a model systematically under or overpredicts the variables of interest. Model bias is determined simply by subtracting the mean predicted value of a variable from the mean observed value, i.e.,

$$B = \bar{O} - \bar{P} \tag{41}$$

where overbars refer to averages.

Dispersion is a measure of the scatter (precision) of model predictions. A model may have no bias and yet still may not be able to accurately predict the individual values of an environmental variable. The Root-Mean-Square-Error (RMSE) is a convenient measure of dispersion:

$$RMSE = \left[\frac{1}{N} \sum_{i=1}^{N} \left(O_i - P_i\right)^2\right]^{1/2} \tag{42}$$

where N is the number of paired observed (O_i) and predicted (P_i) values in the data set.

Correlation coefficients show whether a model-predicted variable responds to forcing (independent variables) in the way that the observed variable does. A model that is biased and lacking in

precision may still be able to predict the response of an environmental variable to external forcing. Although environmental variables may correlate with each other in nonlinear ways, the simple linear correlation coefficient is usually sufficient to determine if model response to forcing is appropriate:

$$r = \frac{\sum_{i=1}^{N} \left(\overline{O} - O_i\right)\left(\overline{P} - P_i\right)}{\left[\sum_{i=1}^{N} \left(\overline{O} - O_i\right)^2 \sum_{i=1}^{N} \left(\overline{P} - P_i\right)^2\right]^{1/2}} \qquad (43)$$

Weber, Buckner and Weber (1982) discuss the methods summarized here in more detail. They also recommend the use of scatter diagrams as a subjective method for analyzing model performance that sometimes reveals model characteristics that were not highlighted by the quantitative tests.

5.2 Lagrangian Model Validation

The Lagrangian model generates temperature time series that are used by the SRL two dimensional finite element model to predict surface temperature distributions in a cooling lake (see Cooper, 1984). If the Lagrangian model is run with time-averaged meteorological data, then the temperature time series decays exponentially to an equilibrium temperature.

The Lagrangian model can be applied directly to stream temperature prediction, because the assumption of a well-mixed fluid is valid. Data presented by Jacobsen et al (1972) from Four Mile, Pen Branch, and Steel Creek on SRP were used to test the model. The results are summarized in Table 1. Although the data are limited,

the mean predictions appear to be fairly good, and the correlation is good, which is to be expected because rapid cooling in the environment of 60 to 70°C water is inevitable. The RMSE is fairly large, but not large enough to prevent use of the model, because much of the error can be attributed to uncertainty about travel time. The travel times given above were estimates by Jacobsen et al (1972). Dye studies conducted by D. W. Hayes of SRL indicate travel times a couple of hours shorter than those given in the table above (personal communication). Stream residence times based on information provided by Murphy and Magoulas (1982) are considerably longer (13 to 24 hours). The Jacobsen et al estimates were used as a compromise.

Additional temperature measurements will be made in the SRP streams in the near future to further validate the Lagrangian model.

5.3 Control Model Validation

5.3.1 Data Bases

Tilly (1981) compiled all available temperature data for Par Pond, which presently receives heated water from the SRP P-Area Reactor via a system of canals and precooler ponds (Fig. 4). The 9 stations in Par Pond where temperature data were gathered are shown in Fig. 4, along with the precoolers. Note that Pond C is separated by the Hot Dam from the rest of Par Pond, and thus is a precooler for the rest of the lake. There is substantial mixing of Pond C water with the colder Par Pond water in the vicinity of station 2 (see Section 3.3).

Temperature measurements were made in Pond C on February 9, April 2, and April 6, 1984. Temperatures in transects across Par Pond were also taken in several places (Fig. 5). These data are given in Tables 2, 3, and 4. Note that transects 1P and 2P in Tables 2 and 4 (also see Fig. 5) found cooler water in the middle and hotter water near both shores. The water in the middle of these transects was 5 to 7°C colder than the water near the edges. This temperature pattern is caused by the upwelling of colder subsurface water which is forced by the strong mixing of Pond C water entering Par Pond. Pond C water enters Par Pond below the surface in the "bubble-up" area. The subsurface entrance is responsible for the strong mixing. Unfortunately, the large temperature gradients in the vicinity of Station 2 make the Tilly data at that station less useful than at the other stations, because Station 2 is only one point, and its exact location is not known.

Three continuous temperature monitoring stations were established in Pond C in July 1984. The first of the three stations is located near the mouth of the canal that carries water from P Reactor and the second station is near the point marked B-3 in Figure 5. The third station is located in the upwelling area of the "bubble-up" and is representative of undiluted water from the lower end of Pond C.

Monthly average and extreme temperatures for Stations 1, 2, 4, 5, 6, 7, and 9 from the Tilly data base are given in Tables 5, 6, 7, 8, 9, 10, and 11. All data are surface data except for the

Station 9 (Par Pond Pumphouse) temperatures, which appear to be representative of averages over about a 6 m (20 ft) layer (Neill and Babcock, 1971). As a result, the Pumphouse temperatures are a little cooler than those from the other stations in Par Pond, even those that are not significantly affected by the P Reactor heat, such as Stations 7, 6 and 5. The Pumphouse temperature measurements are much more numerous that those from the other locations (twice daily for 18.5 years), so they were used for a large part of the model validation described in Section 5.3.2).

Note that in Tables 8, 9, 10, and 11 for stations 5, 6, 7, and 9 the maximum observed temperatures in August exceed 32.2°C (90°F). Even the Station 9 (Pumphouse) data that is representative of average temperatures over a 6 m layer contains readings above 32.2°C. Since the surface data (Stations 5, 6, and 7) are limited (only 10 to 30 observations per month), it is clear that temperatures above 32.2°C will occur in areas of cooling lakes that are only slightly or not at all affected by the heated water from a reactor. These naturally occurring thermal excursions appear to be frequent enough to demand consideration when compliance with regulations that limit lake surface temperatures to 32.2°C (90°F) is required.

5.3.2 Validation with Par Pond Precooler System Data

In order to use the data from the Par Pond canal, precooler, and lake system for model validation, two calculations were performed. In the first calculation, the canal and precooler pond

system including Pond C was treated as a single cooling lake with an area of 227 acres (Jacobsen et al, 1972). The second calculation covered most of Par Pond (see 5.3.3). All of the Pond C area (140 acres) was included in the first calculation, based on EG&G thermal (infrared) photographs and direct measurements (Tables 3 and 4), which show strong penetration of the cold arm by the heated water. Meteorological data was referenced to the actual 6 m observation height, because the precoolers are small. A mixing coefficient (D_v) of 1.5 was assumed, which appears to be a little high for Pond C (see Section 3.3) but which is probably reasonable for Ponds 1 and 2.

Water entering Pond C has passed through about 87 acres of canals and cooling ponds (38% of 227 acres). Temperatures on April 2 and 6, 1984 (see Tables 3 and 4) at the entrance to Pond C were 49.4 and 51.7°C respectively, and the corresponding reactor exit temperatures were 69.1 and 68.8°C. A reactor exit temperature of 67°C was used in the calculations, which is based on average SRP reactor power levels. The computed mean temperature for April at the 35 to 40% point in the precooler system is about 48.5°C, or about 2°C lower than the observed temperature. The transect data in Tables 2, 3, and 4 show temperatures around 45°C in the upper part of Pond C decreasing to 35°C in February and 37 to 39°C in April, in good agreement with predictions (corresponding computed temperature for February is 35.9°C, and for April it is 39.3°C.)

Average temperatures for three weeks in July 1984 from the three continuously operating stations in Pond C are plotted in Figure 6, along with mean computed temperatures for July. The computed temperatures are based on a 10-year meteorological database (1952-1961), and therefore are representative of long-term average Pond C temperatures. The predicted curve falls within the scatter of the data, but it is not known whether the differences between the observations and predictions were caused by the short observation period or model inadequacies. Note that the observed reactor outfall temperature is several degrees higher than the computed outfall temperature. The observed temperatures are measured immediately downstream from the heat exchangers. The temperature decreases by a small amount during the passage of the cooling water from the heat exchangers to the canal outside of P Area.

5.3.3 Validation with Par Pond Data

The Par Pond calculation was performed with an effective cooling area of 1600 acres. All of the cold arm of the lake was excluded from the calculation, based on EG&G thermal (infrared) photographs of the lake, which show little penetration of the warm water from the hot arm. There is relatively little penetration of the thermal plume into the Par Pond cold arm because the plume has cooled to near-ambient temperatures, so the buoyancy force is weak (see Table 7). The mixing coefficient, D_v, was set to 2.6 (see Section 3.3).

Fig. 7 shows mean monthly predicted temperatures for Station 4 (25% of total area) from the control volume model with 31 years (1952 - 1982) of hourly meteorological data as input. The observed and predicted curves agree fairly well, with predicted temperatures a little high, particularly in April and May. Since there were only 10 to 20 observations per month scattered over several years, sampling error may be significant.

Mean monthly predicted temperatures after cooling over 90% of the 1600 acres are compared in Fig. 8 to observed temperatures from Stations 5, 6, 7 and 1970 Cold Dam data presented by Jacobsen et al, (1972). The direct comparison is with Station 6; the other stations were added to show that there is relatively little influence by the P Reactor at any of those locations. The predicted summer temperatures fall within the scatter of the other curves, although the fall observed temperatures run a little higher than the predictions.

In Fig. 9 the observed Pumphouse (Station 9) temperatures are compared to predictions that used a 6.1 m depth instead of the 2.4 m depth that was used in the other calculations. The 6.1 m (20 ft) apparently is representative of the depth over which water at the pumphouse is drawn for use in P Reactor (Neill and Babcock, 1971). All 1600 acres of the computational domain were assumed to be used. It is clear that agreement is very good, however, since this is depth-averaged data, its validity for testing the ability of the control volume model to predict surface temperature for the proposed L-Lake is not perfect.

Keeping the nature of the Pumphouse data in mind, it is nevertheless appropriate to perform other statistical tests with it, because it is the only large data base available (18.5 years of twice daily observations). Time series of observed and predicted monthly mean temperatures were developed for the years 1961 through 1979 (July) and 1962 through 1979 (January). For July, the correlation coefficient was 0.63 (0.01 significance level), the RMSE was 1.0°C, and the bias was -0.2°C (28.5°C observed, 28.7°C predicted. For January, the correlation was 0.78 (0.001 significance level), the RMSE was 2.0°C, and the bias was + 1.5°C (11.3°C observed, 9.8°C predicted). Again, surface monthly temperature predictions may not be quite so good.

Figs. 10 and 11 show observed and predicted daily temperature time series for the Pumphouse for June through August of 1977 (Fig. 10) and 1973 (Fig. 11). For 1977, the correlation was 0.77, the RMSE was 1.0, and the bias was -0.5°C (28.6°C observed, 29.1°C predicted). For 1973, the correlation was 0.81, the RMSE was 1.2°C, and the bias was +0.8°C (29.0°C observed, 28.2°C predicted). It is unlikely that daily surface temperatures can be predicted this accurately, because the effects of wind direction shifts on surface temperatures will probably be more pronounced than direction shift effects will be for temperatures averaged over 6.1 m. Neill and Babcock (1971) attributed 2 to 3°C changes in temperatures over short time periods to changes in wind direction.

6. Observed and Computed Extremes

The previous section did not address observed and computed maximum temperatures in Par Pond. Maximum temperatures in the proposed L Area cooling lake are of particular concern, because the 32.2°C (90°F) isotherm must not cover more than half of the lake over some specified averaging time. As discussed, in Section 5.3.1, surface and even depth-averaged temperatures sometimes exceed 32.2°C in areas of Par Pond that are affected slightly or not at all by hot water from P Reactor.

Maximum temperatures reported from Stations 5, 6, 7, and 9 are graphed in Figure 12, along with computed maximum temperatures at the lower (dam) end of the proposed L Lake. Observed maxima range as high as 33°C; the computed maximum was 35°C. The computed mean temperature at the lower end of L Lake during July and August is 29.2°C, which is close to the equilibrium temperature. Since the observed curves in Figure 12 are from limited or depth-averaged data bases, the predicted maximum surface temperatures in areas of the lake only slightly affected by heated reactor water appear reasonable. Neill and Babcock (1971, p.45) reported a July surface temperature of 34.5°C in Par Pond near the Pumphouse (Station 9). These naturally-occurring thermal excursions are transient, but they clearly occur in significant numbers during the summer.

7. Conclusions

The model validation described in this document indicates that the methods described here and by Cooper (1984) for predicting the performance of the proposed L Area cooling lake are reliable. The models will be further tested as more temperature data from the Par Pond system are gathered.

Extensive observations from the Par Pond system show that lake surface temperatures exceeding 32.2°C (90°F) are attained occasionally in the summer in areas where there is little or no heating from the P-Area Reactor. Regulations which restrict lake surface temperatures to less than 32.2°C should be structured to allow for these naturally-occurring thermal excursions.

References

Adams, E. E., K. R. Helfrich, D. R. F. Harleman, and A. L. Godbey, 1980: Evaluation of models for predicting evaporative water loss and hydrothermal performance in cooling impoundments. R. M. Parsons Laboratory for Water Resources and Hydrodynamics and Energy Laboratory. M.I.T.

Brutsaert, W. F., 1982: Evaporation and the Atmosphere. Reidel, 299 pp.

Cooper, R. E., 1984: Estimates of temperature distributions in the proposed L-Area cooling pond and related thermal effect in streams. USDOE DPST-84-479. Savannah River Laboratory.

Firstenburg and Fisher, 1980: An investigation of cooling lakes for the closed cycle operation of electric generating stations. NUS Corporation.

Fisher, H. B., 1967: The mechanics of dispersion in natural streams. J. of the Hydraulic Division, ASCE, Vol. 93, No. HY6, Proc. Paper 5592.

Garrett, A. J., 1977: A comparison of the observed longwave radiation flux to calculations based on Kondratyev's and Brunt's methods. Arch. Met. Geoph. Biokl. Ser.B., 25, 127-134.

Garrett, A. J., 1978: Numerical simulations of atmospheric convection over the southeastern U. S. in undisturbed conditions. University of Texas Atmospheric Science Group Rep. No. 47, 356 pp.

Garrett, A. J. 1980: Orographic cloud over the eastern slopes of Mauna Loa Volcano, Hawaii, related to insolation and wind. Mon. Wea. Rev., 108, 931-941.

Garrett, A. J., 1982: A parameter study of interactions between convective clouds, the convective boundary layer, and a forested surface. Mon. Wea. Rev., 110, 1041-1059.

Irwin, J. S., 1979: A theoretical variation of the wind profile power law exponent as a function of surface roughness and stability. Atmospheric Environment. 13, 191-194.

Jacobsen, W. R., R. J. Brown, E. W. Rabon, and L. J. Tilly, 1972: Thermal discharges from the Savannah River Plant. USDOE DPST-72-428, Savannah River Laboratory.

References, Contd

Johnston, B. S., and M. A. McLain, 1984: Experimental model of L-Area outfall. USDOE DPST-84-726. Savannah River Laboratory.

Jirka, G. H., M. Watanabe, K. H. Octavio, C. F. Cerco, and D. R. F. Harleman, 1978: Mathematical predictive models for cooling ponds and lakes, Part A. Ralph M. Parsons Laboratory for Water Resources and Hydrodynamics. Report No. 238, Dept. Civil Eng., MIT, 199 pp.

Jirka, G. H., and M. Watanabe, 1980: Thermal structure of cooling ponds. J. of Hydraulics Div., ASCE, 106, 701-715.

Kondratyev, K. Ya., 1969: Radiation in the Atmosphere. New York, Academic Press, 915 pp.

Louis, J. F., 1979: A parametric model of vertical eddy fluxes in the atmosphere. Boundary Layer Meteor., 17, 187-202.

Magoulas, V. E., and C. E. Murphy, Jr., 1982: Processes influencing cooling of reactor effluents. USDOE DPST-82-617. Savannah River Laboratory.

National Oceanic and Atmospheric Administration, 1974: Climates of the States, Volume I, U. S. Dept. of Commerce.

Neill, J. S., and D. F. Babcock, 1971: The dissipation of reactor heat at the Savannah River Plant. USDOE DP-1274.

Ryan, P. T., and D. R. F. Harleman, 1973: An analytical and experimental study of transient cooling pond behavior. Dept. of Civil Engineering, MIT, R. M. Parsons Laboratory for Water Resources and Hydrodynamics. Tech. Report 161.

Tilly, L. J., 1981: Limnological database for Par Pond: 1959-1980. USDOE DP-1575.

Weber, A. H., M. R. Buckner, and J. H. Weber, 1982: Statistical performance of several mesoscale atmospheric dispersion models. J. Appl. Meteor., 21, 1633-1644.

Table 1

Lagrangian Model Validation

	Four Mile	Pen Branch	Steel Creek
depth (m)	1.0	1.2	1.0
distance to swamp (km)	11	9	11
travel time (hrs)	10	8	13

Number of data points = 18

Mean Observed temperature = 42.6°C

Mean Predicted Temperature = 43.5°C

Bias = −0.9°C

Root Mean Square Error = 3.6°C

Correlation Coefficient = 0.90

Table 2

Canal and Pond Study
February 9, 1984 0930-1100

Location		Air Temp. °C	RH%	Wind Speed	Wind Direction	Sky Cover %	Water Temp. 1 cm	Remote IR (Infrared) Temp.
P Area, Road F		10	45	1-2 m/s	SW	0	62	65
Pond 2	A						59	58
	B						55.5	53
	C						56	55.5
Pond 4/5	A						54.4	53
	B						49	46
	C						48	48
Transect 1	PA						24.4	24.5
	B						14.6	14.2
	C						15.3	15.3
	D						14.7	14.3
	E						23.2	23.5
	2PA						21.4	25.0
	B						21.3	21.0
	C						17.1	16.0
	D						18.0	18.0
	E						19.5	19.5
	3PA						17.4	Missing
	B						17.7	Missing
	C						18.4	Missing
	D						18.9	Missing
	E						17.6	Missing

Table 2 contd

Canal and Pond Study
February 9, 1984 0930-1100

Location		Air Temp. °C	RH%	Wind Speed	Wind Direction	Sky Cover %	Water Temp. 1 cm	Remote IR (Infrared) Temp.
Pond C	4A						>40	Missing
	B						>40	Missing
	C						38.5	Missing
	D						36.8	Missing
	E						34.7	Missing

Table 3a

Par Pond Temperature Study
April 2, 1984 1035 - 1330

Canal Entrance 69.1°C
Canal Exit 51.7°C

Transect Location	Remote IR (Infrared) Temp.	0.15 m	0.31 m	0.62 m	1 m	2 m	3 m	4 m	5 m	6 m
3PA	24.6	21.2	25.2	24.7	24.2	19.8	18.7	18.2	17.9	17.8
3PB	24.0	25.4	24.6	24.4	23.9	21.2	18.8	18.2	18.0	17.7
3PC	24.6	25.9	25.9	25.5	24.7	21.9	19.0	18.3	18.0	17.7
3PD	26.2	27.0	26.0	24.2	23.6	20.9	18.5	18.2	17.8	17.7
3PE	25.5	26.5	26.2	25.7	23.8	20.2	19.2	Bottom		
5PA	22.1	23.0	23.1	22.1	20.7	19.7	18.9	18.2	17.9	17.7
5PB	22.3	23.0	22.9	22.4	21.7	19.5	18.3	18.0	17.7	17.6
5PC	22.3	23.0	22.7	22.7	22.7	19.5	18.3	17.9	17.7	17.6
5PD	22.0	23.2	23.1	22.9	23.3	18.8	18.4	17.9	17.0	Bottom
5PE	22.7	23.0	22.9	23.0	23.0	18.7	Bottom			
6PA	19.0	19.7	19.7	19.7	19.7	19.6	18.8	17.9	17.5	17.3
6PB	18.9	19.5	19.5	19.5	19.4	19.1	18.8	18.2	17.5	17.0
6PC	18.7	19.5	19.5	19.4	19.4	19.0	18.7	18.3	17.8	17.0
6PD	18.6	19.3	19.3	19.3	19.3	18.8	18.5	18.2	17.7	17.2
6PE	18.6	19.2	19.2	19.1	18.9	18.7	18.5	18.4	17.4	17.0
7PA	18.9	19.7	19.7	19.7	19.7	19.7	19.6	18.0	17.6	Bottom
7PB	18.6	19.5	19.5	19.5	19.4	19.4	18.9	18.1	17.2	Bottom
7PC	18.7	19.5	19.5	19.4	19.4	19.2	18.7	18.2	17.5	17.1
7PD	18.6	19.5	19.4	19.2	19.1	18.8	18.4	18.2	18.0	17.3
7PE	18.2	19.2	19.1	18.8	18.6	18.5	18.3	18.2	18.0	17.9
Ambient	18.0	18.7	18.7	18.6	18.5	18.4	18.4	18.0	18.0	17.7

Table 3b

Par Pond Temperature Study
April 2, 1984 1035 - 1330

Canal Entrance 69.1°C
Canal Exit 51.7°C

Transect Location	Remote IR (Infrared) Temp.	0.15 m	0.31 m	0.62 m	1 m	2 m	3 m	4 m	5 m	6 m
4C2A	39.0	41.1	41.0	41.0	40.4	39.7	39.2	37.5	Bottom	
4C2B	39.0	40.6	40.6	40.5	40.4	40.2	39.3	38.9	38.3	Bottom
4C2C	38.5	41.7	41.6	41.4	41.1	40.0	39.3	38.8	38.3	37.7
4C2D	40.0	44.8	44.7	42.5	41.9	39.8	39.4	39.1	38.6	36.9
4C2E	40.0	44.0	43.9	43.4	41.7	40.0	Bottom			
4C3A	36.5	39.6	39.6	39.6	39.,6	39.4	Bottom			
4C3B	37.5	39.6	39.6	39.6	39.5	39.3	39.0	38.7	Bottom	
4C3C	37.5	39.5	39.5	39.5	39.5	39.3	39.0	38.8	38.4	37.5
4C3D	37.5	39.4	39.4	39.4	39.4	39.4	39.2	38.8	38.6	38.2
4C3E	37.5	39.5	39.5	39.5	39.4	39.2	Bottom			
4C4A	43.5	47.3	47.1	42.2	41.2	39.6	39.4	38.2	Bottom	
4C4B	45.0	47.5	47.2	43.9	41.8	39.8	39.4	38.8	37.1	Bottom
4C4C	41.0	44.7	44.6	43.9	4.04	40.4	39.0	37.8	35.6	Bottom
4C4D	38.0	42.1	42.1	42.0	41.9	40.6	37.7	Bottom		
4C4E	36.5	40.4	40.3	39.6	37.0	Bottom				

Table 4a

Par Pond Transects
April 6, 1984 0930-1330

Canal Entrance - 68.8°C 70.0°IR
Canal Exit - 49.4°C 49.0°IR
Bubble up T° - 36.5°C

Transect Location	Remote IR (Infrared) Temp.	0.15 m	0.31 m	0.62 m	1 m	2 m	3 m	4 m	5 m	6 m
1PA	29.0	30.3	27.0	26.4	24.0	20.5	19.0	18.2	Bottom	
1PB	22.0	21.9	21.9	21.9	21.8	19.6	18.7	18.1	17.9	17.7
1PC	22.5	23.1	22.8	22.4	21.3	20.0	18.5	18.2	Bottom	
1PD	22.3	22.1	22.1	21.9	21.5	20.6	18.4	18.2	Bottom	
1PE	29.6	28.6	28.6	25.7	26.9	22.3	Bottom			
2PA	27.6	25.4	22.1	21.2	20.8	18.4	18.6	Bottom		
2PB	27.0	24.8	24.2	22.9	22.0	18.7	18.9	18.4	18.3	18.0
2PC	22.2	22.2	22.3	22.3	22.3	20.1	18.5	18.2	18.1	18.0
2PD	27.0	26.9	26.6	25.0	22.8	21.1	18.6	18.3	18.1	18.0
2PE	27.0	26.7	26.6	26.5	25.5	19.8	18.6	Bottom		
3PA	19.0	18.6	18.6	18.5	18.6	18.2	18.4	18.3	18.0	17.6
3PB	21.2	21.5	21.6	21.6	21.2	19.3	18.5	18.0	17.7	17.6
3PC	24.5	24.6	24.6	23.5	23.3	19.2	18.5	18.0	17.8	17.8
3PD	24.5	24.5	24.4	24.2	22.2	19.2	18.7	18.1	17.8	17.7
3PE	24.5	24.4	24.5	24.6	24.5	19.2	18.5	Bottom		
4PA	21.3	21.2	21.1	21.1	21.1	21.0	19.5	Bottom		
4PB	20.2	20.5	20.5	20.5	20.5	20.4	20.2	19.3	18.7	17.8
4PC	19.2	19.6	19.6	19.6	19.6	19.5	19.5	19.3	19.1	17.8
4PD	19.2	19.5	19.5	19.5	19.5	19.4	19.4	19.3	18.7	18.1
4PE	19.5	19.7	19.8	19.7	19.7	19.5	Bottom			
Ambient A	19.0	18.8	18.8	18.8	18.8	18.8	18.8	18.8	18.8	18.8
Ambient B	17.5	17.1	17.1	17.1	17.1	17.1	17.1	17.1	17.1	17.1

Table 4b

Par Pond Transects
April 6, 1984 1040-1140

Canal Entrance - 68.8°C
Canal Exit - 49.4°C

Transect Location	Remote IR (Infrared) Temp.	0.15 m	0.31 m	0.62 m	1 m	2 m	3 m	4 m	5 m	6 m
Pond C										
4C1A	38.2	38.3	38.2	38.0	37.5	37.1	36.9	36.2	Bottom	
4C1B	38.0	39.2	39.1	39.0	38.8	37.2	36.9	36.6	36.2	35.4
4C1C	38.0	38.3	38.3	38.2	38.1	37.5	37.2	36.4	36.0	Bottom
4C1D	38.0	38.0	37.9	37.9	37.8	37.6	37.0	36.9	36.5	35.6
4C1E	40.0	37.5	37.5	37.5	37.5	37.4	37.4	37.3	37.1	36.5
4C2A	38.0	39.8	39.7	39.7	39.5	38.0	Bottom			
4C2B	38.0	39.9	39.9	39.8	39.3	37.8	36.7	36.5	36.2	36.0
4C2C	38.0	39.1	39.1	39.0	38.6	38.0	37.1	36.8	36.6	36.4
4C2D	38.0	38.6	38.6	38.6	38.5	38.2	37.0	36.9	36.8	36.5
4C2E	38.0	38.6	38.6	38.5	39.0	38.2	36.6	Bottom		
4C3A	38.0	37.3	37.3	37.3	37.2	37.2	36.7	Bottom		
4C3B	38.0	37.5	37.5	37.5	37.4	37.3	37.2	37.2	37.2	36.9
4C3C	44.0	37.5	37.5	37.5	37.5	37.4	37.4	37.3	37.1	36.5
4C3D	39.0	37.5	37.5	37.5	37.5	37.5	37.5	37.5	37.4	37.4
4C3E	38.0	37.2	36.9	36.6	36.2	35.2	Bottom			
4C4A	39.0	42.5	41.7	41.0	37.4	36.9	36.7	36.6	Bottom	
4C4B	38.2	40.0	39.9	39.8	38.9	37.0	36.7	36.2	35.5	34.5
4C4C	46.0	38.5	38.4	38.3	38.2	37.6	36.9	35.2	33.9	Bottom
4C4D	38.0	37.2	37.2	37.1	36.9	36.4	34.9	32.8	Bottom	
4C4E	38.0	35.9	35.9	35.8	35.4	34.5	31.6	Bottom		

Table 4b contd

Par Pond Transects
April 6, 1984 1153-1210

Canal Entrance - 68.8°C
Canal Exit - 49.4°C

Transect Location	Remote IR (Infrared) Temp.	0.15 m	0.31 m	0.62 m	1 m	2 m	3 m	3.5 m
Pond C								
4C5A	> 35	44.2	44.0	42.5	37.1	Bottom		
4C5B	> 35	43.2	42.3	41.5	37.2	36.8	Bottom	
4C5C	> 35	44.6	43.2	40.1	37.2	36.9	36.6	36.3
4C5D	> 35	43.8	40.0	37.3	37.2	37.0	Bottom	
4C5E	> 35	40.4	38.8	37.7	37.7	Bottom		

Table 5

Station 1 Means and Extremes

Month	Mean Temperature (°C)	Standard Deviation (°C)	Maximum	Minimum	Number of Observations
1	16.63	4.74	23.90	10.50	7
2	17.01	2.85	23.00	12.30	20
3	20.23	2.50	25.30	15.60	24
4	23.19	2.60	28.40	18.40	21
5	26.17	2.08	30.30	22.70	24
6	29.76	2.25	33.20	26.10	14
7	31.99	1.50	33.90	29.10	11
8	32.01	1.53	35.60	28.60	21
9	30.17	1.37	32.50	27.50	15
10	25.66	2.48	30.60	21.50	17
11	20.65	2.68	26.50	17.20	13
12	19.94	3.63	24.60	14.20	8

Table 6

Station 2 Means and Extremes

Month	Mean Temperature (°C)	Standard Deviation (°C)	Maximum	Minimum	Number of Observations
1	17.67	3.34	24.50	12.20	21
2	17.07	3.43	28.50	13.50	19
3	20.15	3.71	29.00	14.20	21
4	24.10	3.15	32.50	19.90	21
5	28.06	2.86	33.40	24.00	18
6	31.24	1.94	35.20	27.40	22
7	32.82	1.80	36.00	28.60	23
8	32.36	1.85	35.90	28.00	19
9	31.15	2.38	36.00	26.90	20
10	26.20	2.24	30.00	22.20	21
11	21.81	3.70	29.20	16.10	18
12	18.17	2.68	21.40	12.20	23

Table 7

Station 4 Means and Extremes

Month	Mean Temperature (°C)	Standard Deviation (°C)	Maximum	Minimum	Number of Observations
1	15.79	3.66	23.00	12.00	8
2	16.38	2.54	23.40	11500	20
3	18.97	2.60	24.40	14.60	23
4	22.08	2.36	26.60	18.20	22
5	25.40	2.38	30.40	21.20	23
6	29.96	1.95	33.00	26.50	16
7	31.82	1.25	33.80	29.00	13
8	31.66	1.80	35.60	28.50	23
9	28.93	2.51	32.30	21.20	18
10	24.78	2.17	29.20	21.40	19
11	19.68	2.98	26.10	13.30	17
12	18.21	3.26	24.50	11.30	10

Table 8

Station 5 Means and Extremes

Month	Mean Temperature (°C)	Standard Deviation (°C)	Maximum	Minimum	Number of Observations
1	14.33	2.20	19.60	9.00	29
2	13.20	2.12	19.20	10.20	28
3	14.98	2.72	22.30	10.20	42
4	20.88	2.18	24.60	16.30	35
5	25.08	2.16	29.30	21.40	31
6	27.54	1.41	32.20	25.00	31
7	29.29	1.14	31.70	27.50	33
8	29.84	1.36	33.00	26.50	28
9	27.32	1.39	30.00	24.60	27
10	23.09	2.13	28.20	19.40	33
11	19.01	1.75	22.70	13.70	27
12	15.01	1.70	19.00	11.00	31

Table 9

Station 6 Means and Extremes

Month	Mean Temperature (°C)	Standard Deviation (°C)	Maximum	Minimum	Number of Observations
1	14.53	2.64	20.00	10.90	12
2	14.01	2.07	17.10	10.80	10
3	16.81	2.22	22.60	13.00	13
4	20.79	1.96	24.50	17.70	12
5	23.61	1.50	26.10	21.00	10
6	27.65	1.00	29.50	25.60	11
7	29.41	1.17	31.20	27.60	14
8	29.78	1.20	32.30	28.10	10
9	27.73	1.49	29.40	25.00	10
10	22.64	2.27	26.70	19.80	9
11	19.29	1.68	22.80	14.30	8
12	14.16	2.14	18.10	11.20	10

Table 10

Station 7 Means and Extremes

Month	Mean Temperature (°C)	Standard Deviation (°C)	Maximum	Minimum	Number of Observations
1	14.53	2.59	19.60	10.30	13
2	14.04	2.16	19.20	10.90	12
3	17.31	1.99	21.80	13.00	13
4	20.68	2.47	25.00	16.00	12
5	24.51	1.66	27.50	21.90	10
6	28.56	1.37	30.60	25.50	11
7	30.02	1.12	32.20	28.20	14
8	29.92	1.54	32.50	27.60	10
9	27.06	1.23	29.10	25.00	10
10	22.93	2.61	27.30	19.50	9
11	19.04	2.69	22.50	14.10	8
12	14.47	2.36	17.60	11.00	10

Table 11

Station 9 Means and Extremes

Month	Mean Temperature (°C)	Standard Deviation (°C)	Maximum	Minimum	Number of Observations
1	11.18	2.59	19.40	5.30	1090
2	11.20	2.18	19.80	5.80	962
3	14.49	2.34	23.30	2.80	1112
4	19.00	2.35	24.40	12.80	1075
5	23.43	2.22	31.70	11.40	1094
6	26.51	2.17	32.20	17.20	1074
7	28.53	1.41	32.80	22.80	1107
8	28.68	1.92	32.30	21.10	1120
9	27.14	2.14	30.60	17.80	1090
10	22.62	2.55	29.90	11.70	1146
11	17.39	2.63	24.40	8.90	1105
12	13.16	2.60	20.00	3.30	1171

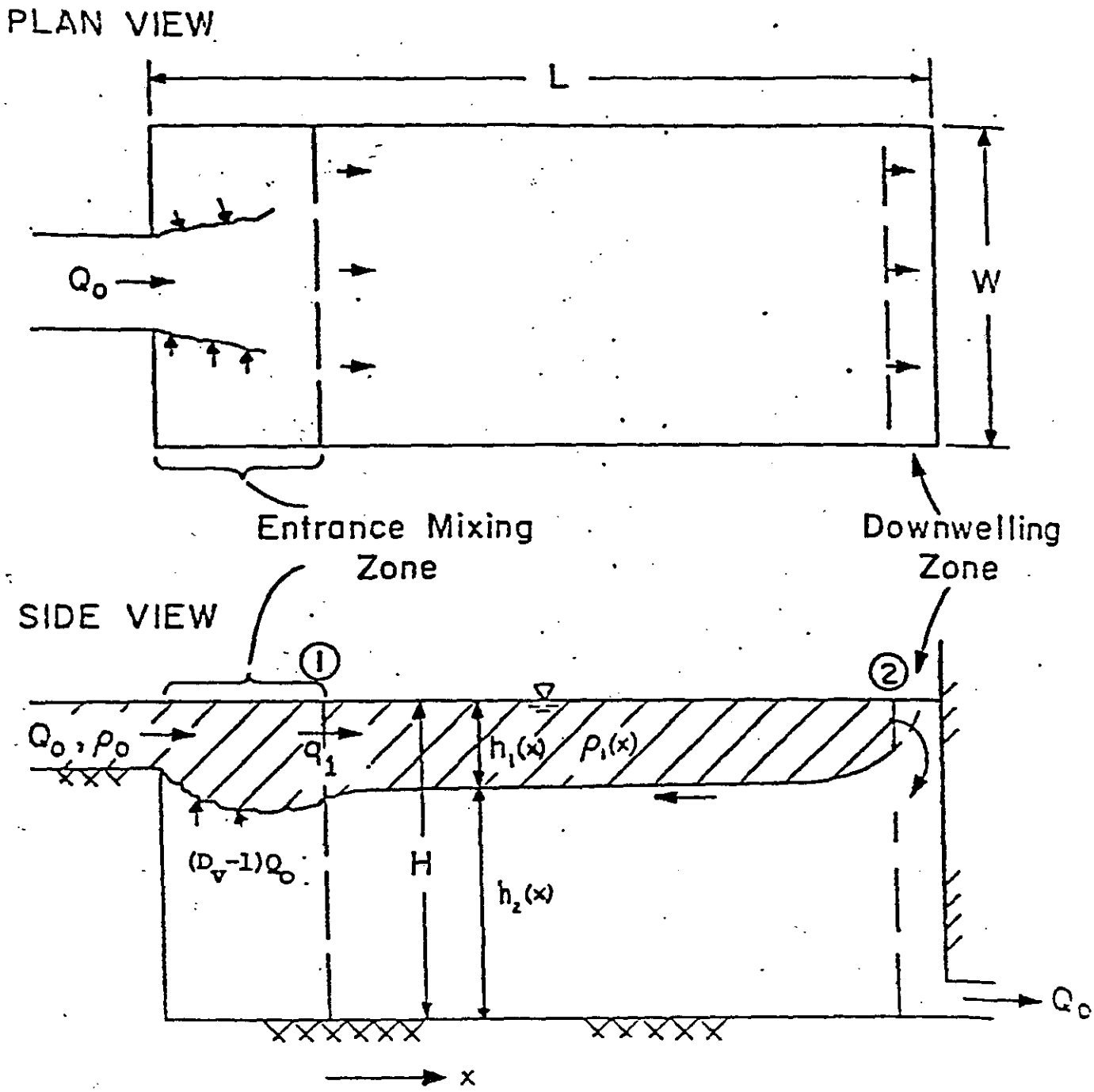

Figure 1. : Schematics of the Thermal Structure of a Deep Cooling Pond (Entrance Mixing and Downwelling Zones are a Small Portion of Total Pond Area) (Adapted from Jirka et al, 1978)

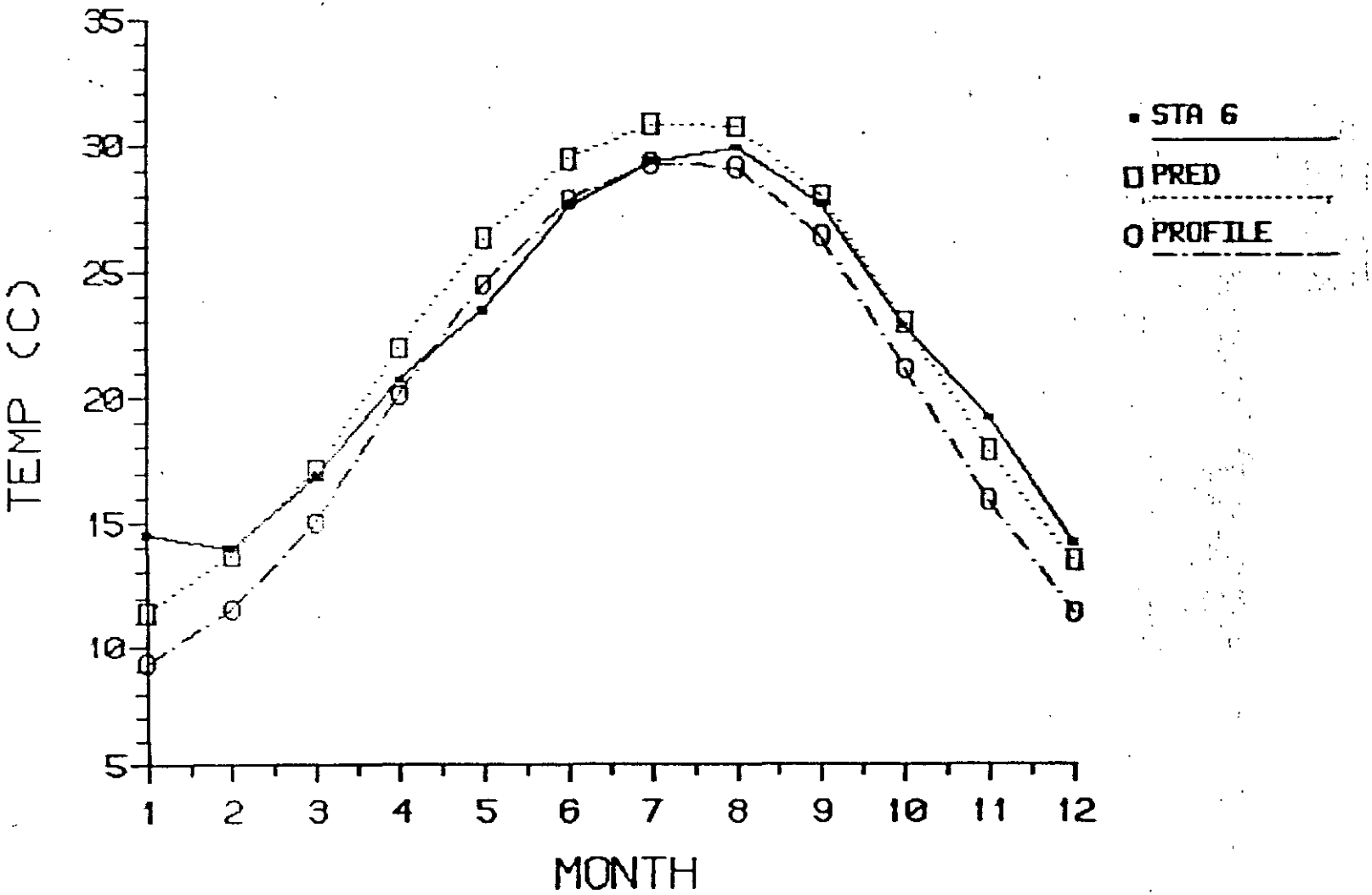

Figure 2. Results of model sensitivity tests with (PROFILE) and without (PRED) wind speed corrections from 6 to 50 m.

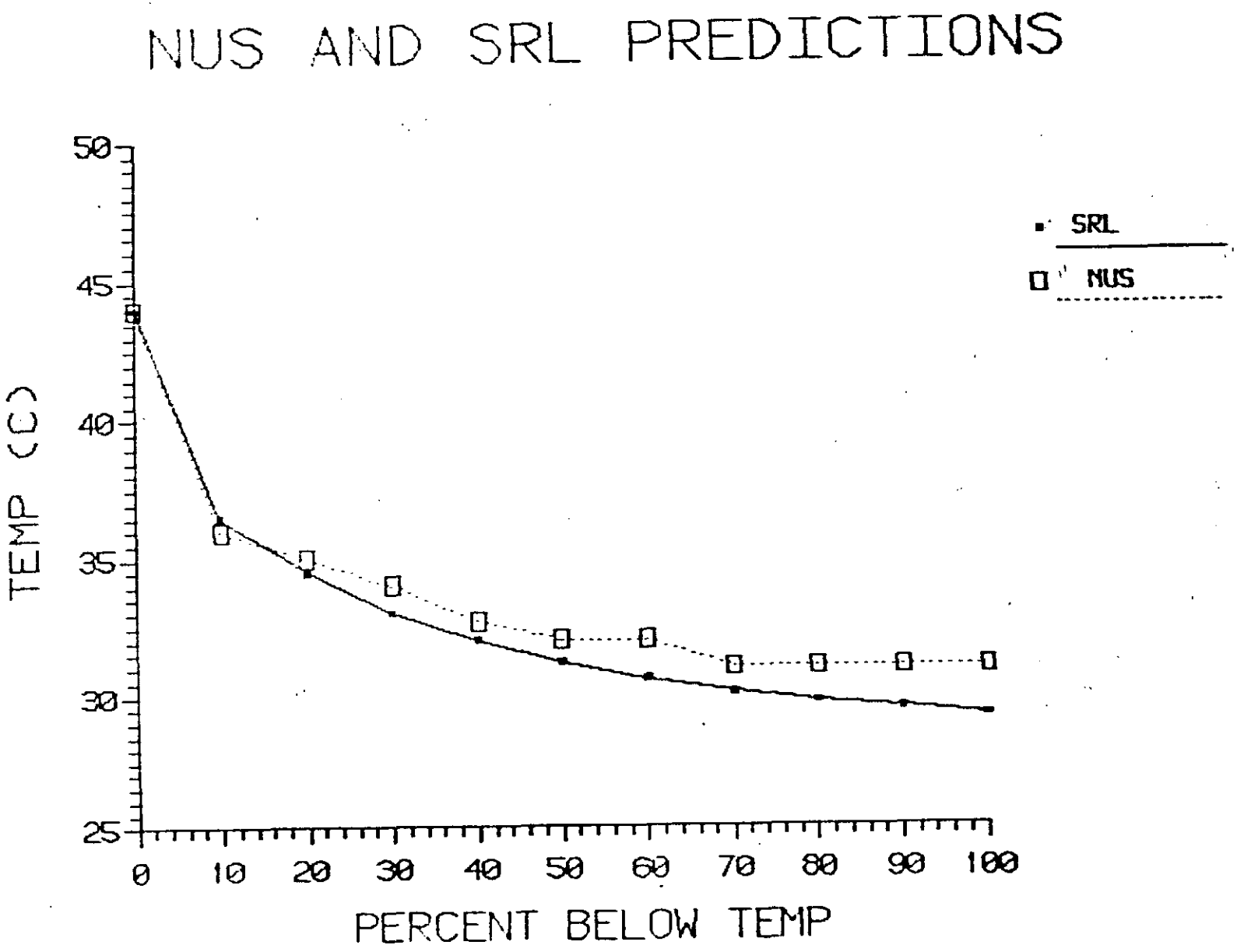

Figure 3a. Comparison of Nuclear Utility Services (NUS) and Savannah River Laboratory (SRL) predictions of mean seasonal surface temperatures in the proposed L Area Lake. (Summer)

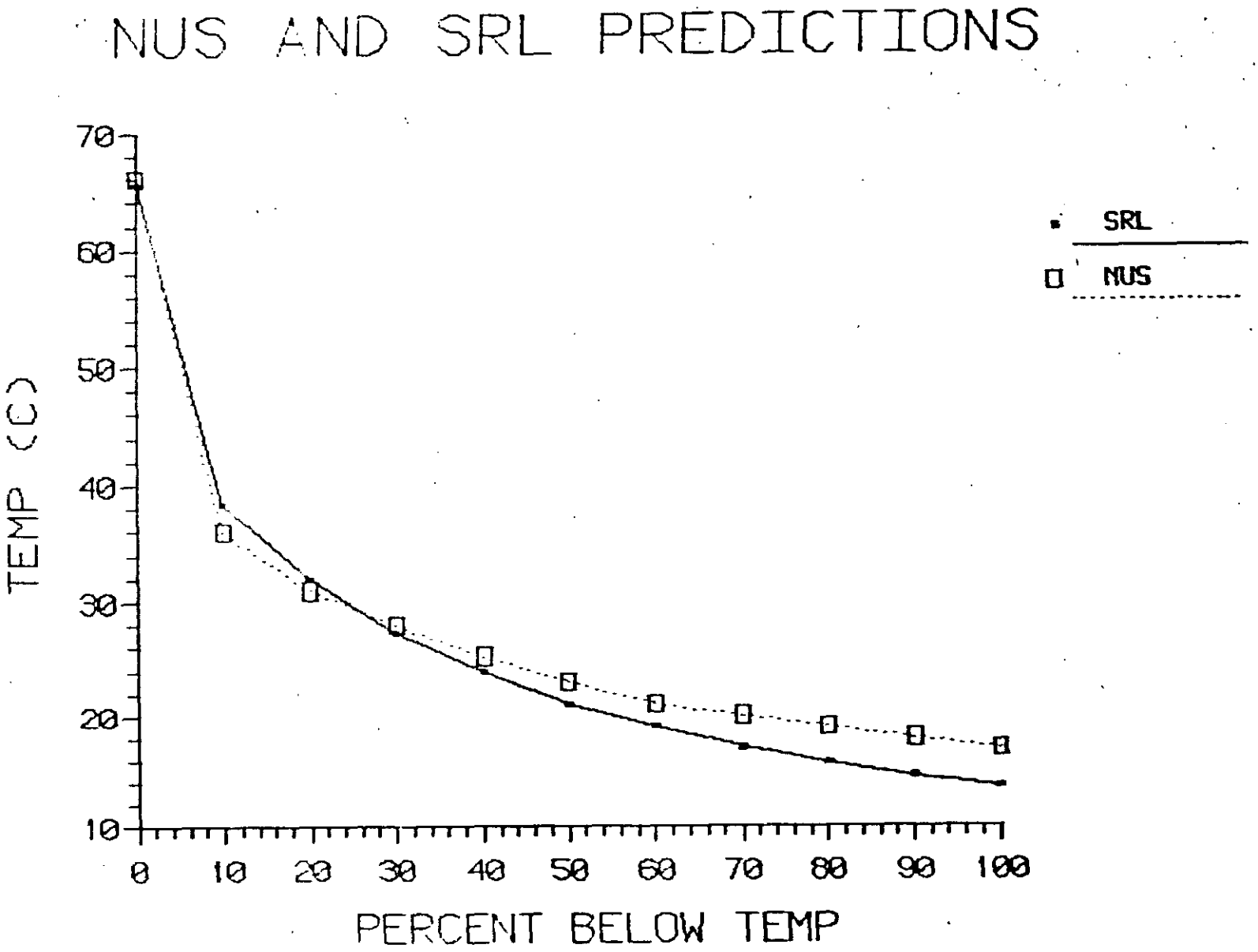

Figure 3b. Comparison of Nuclear Utility Services (NUS) and Savannah River Laboratory (SRL) predictions of mean seasonal surface temperatures in the proposed L Area Lake. (Winter)

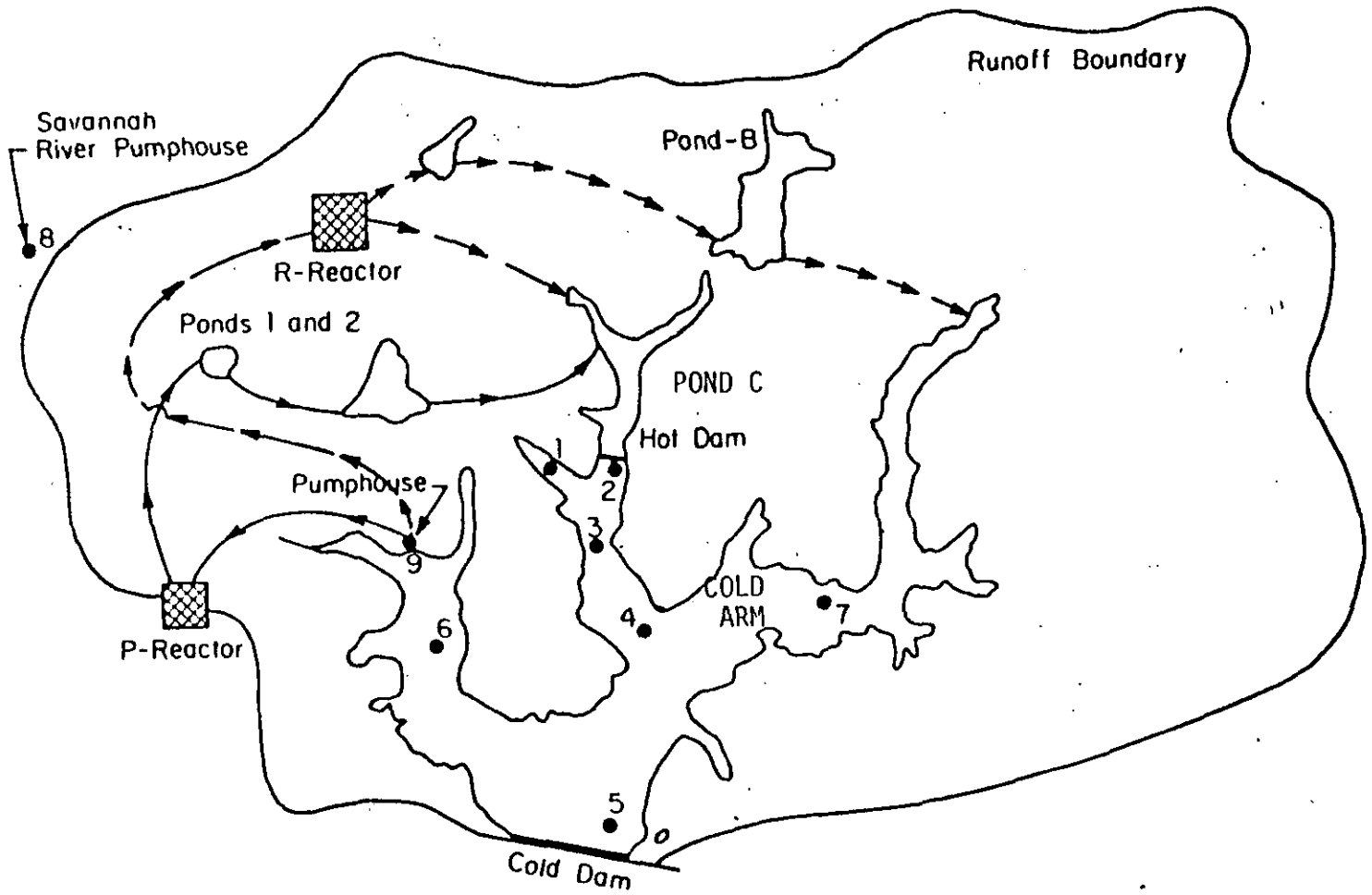

P-Reactor Pumping Flow Path

Previous R-Reactor Pumping Flow Path

FIGURE 4. Par Pond Sampling Stations (1 through 9) and Rainfall-Runoff Area

Figure 5. Transect locations for Tables 2, 3, and 4.

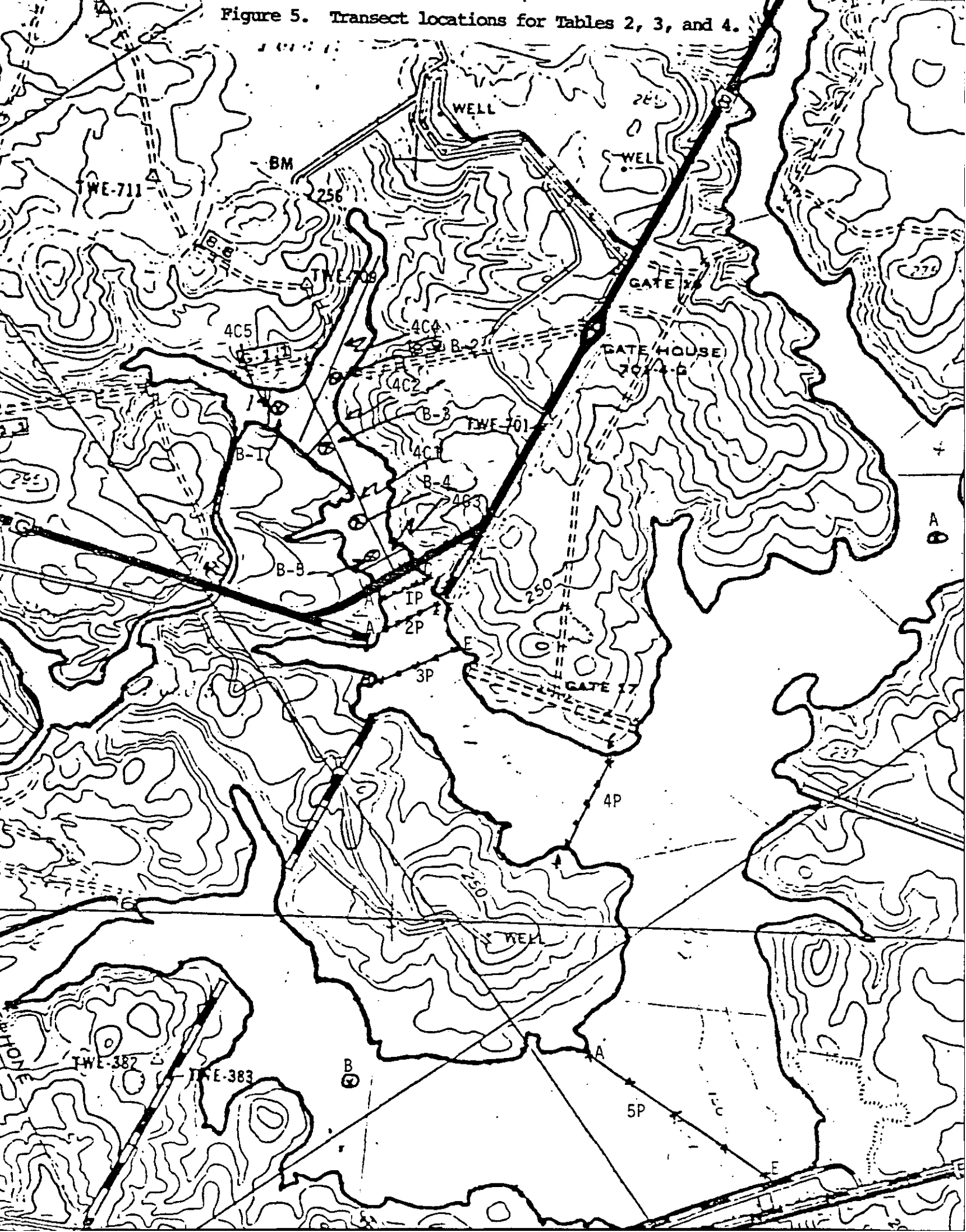

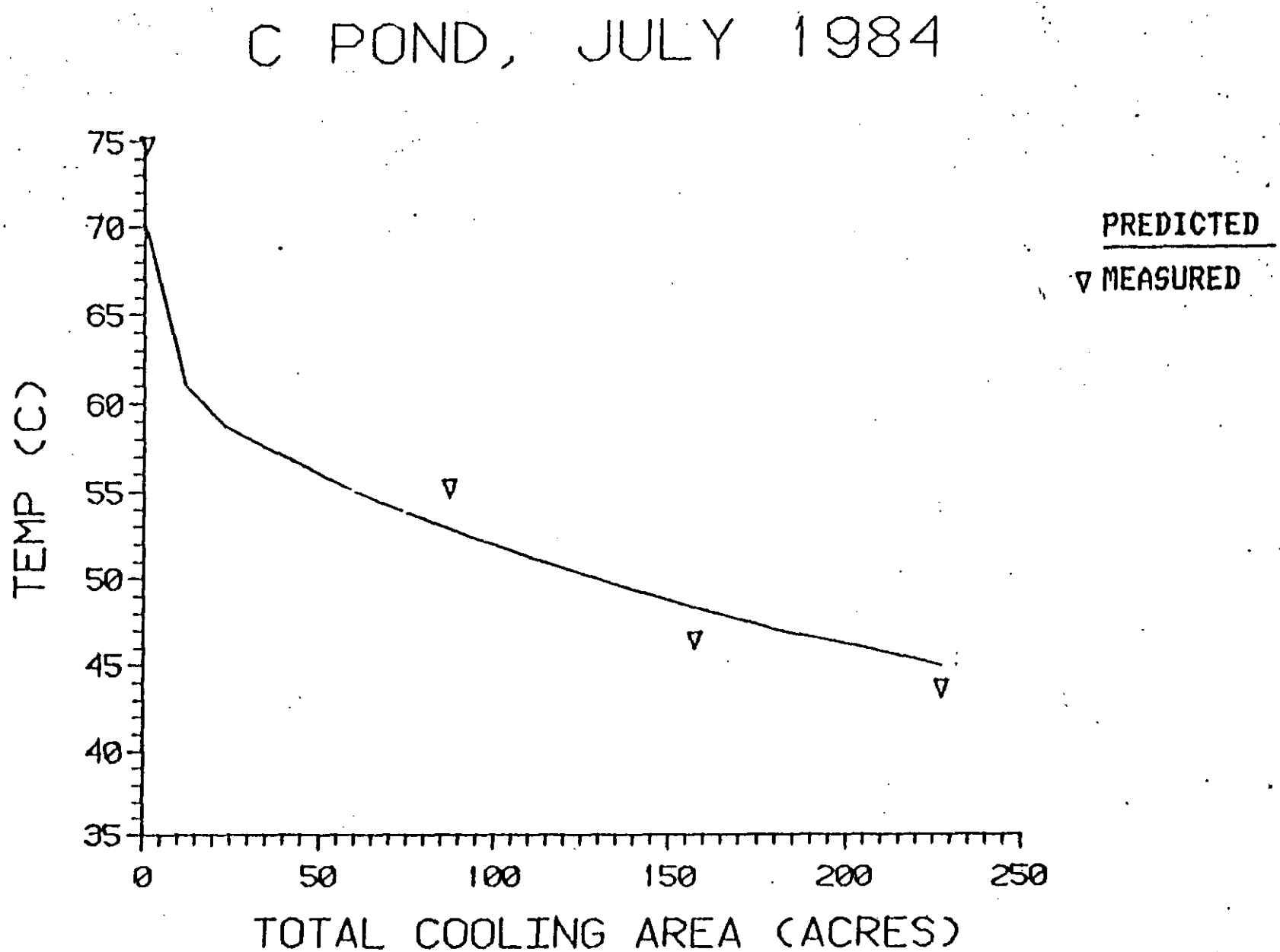

Figure 6. Predicted and measured surface temperatures in Pond C. Total cooling area includes precoolers upstream from Pond C.

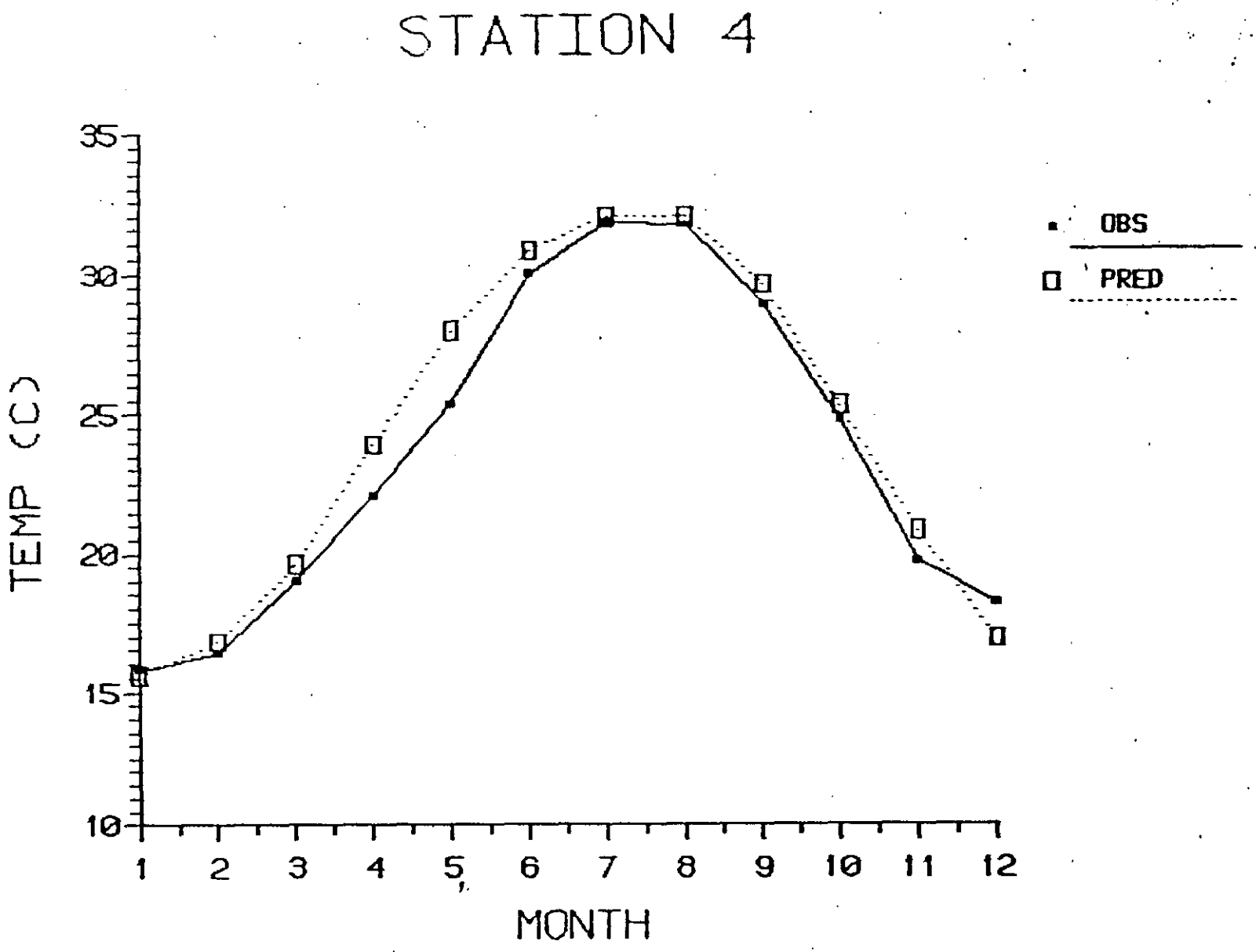

Figure 7. Predicted (PRED) and observed (OBS) monthly mean surface temperatures at Station 4 in Par Pond.

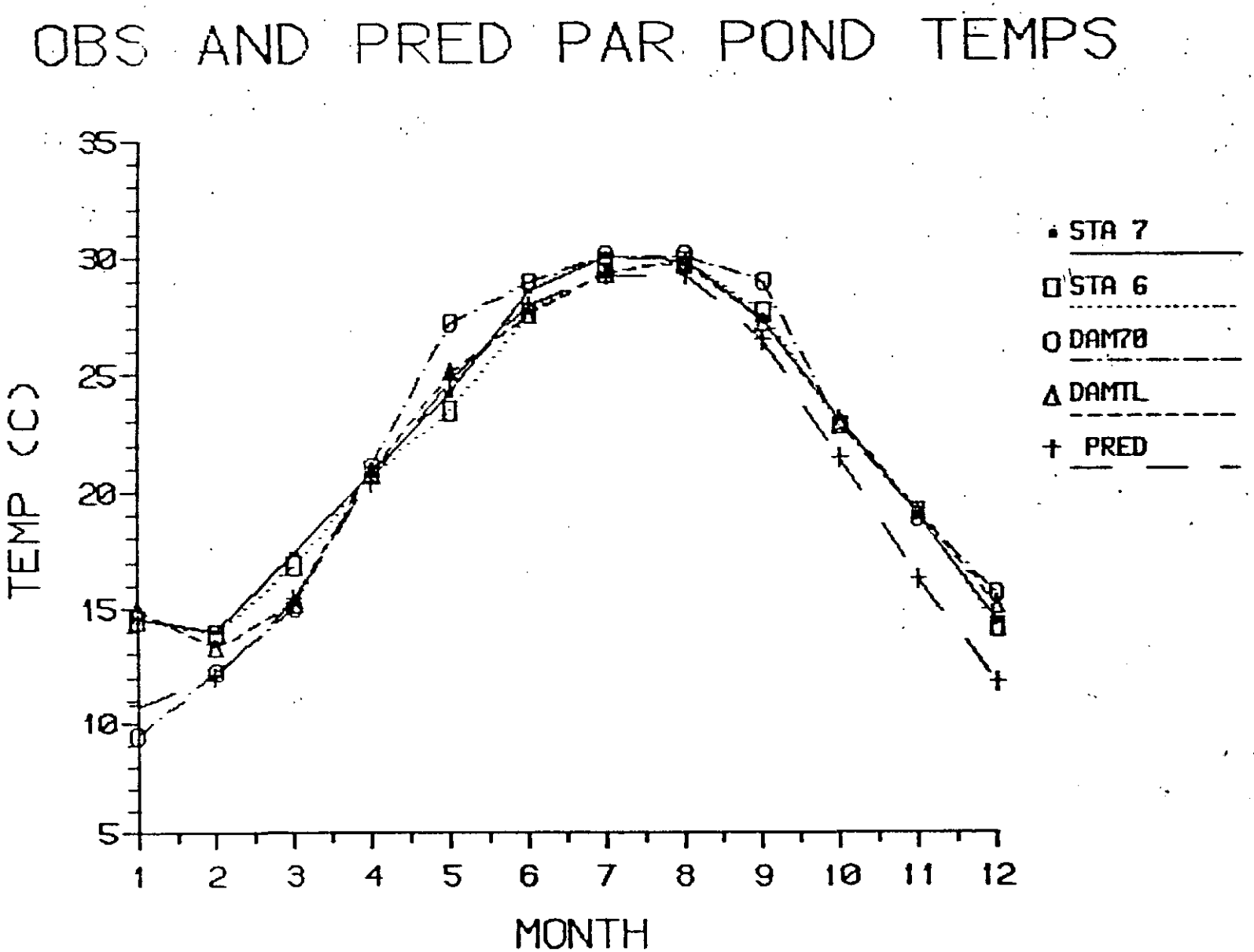

Figure 8. Predicted (PRED) and observed monthly mean surface temperaturese at several stations in Par Pond that are relatively unaffected by P Reactor heated water.

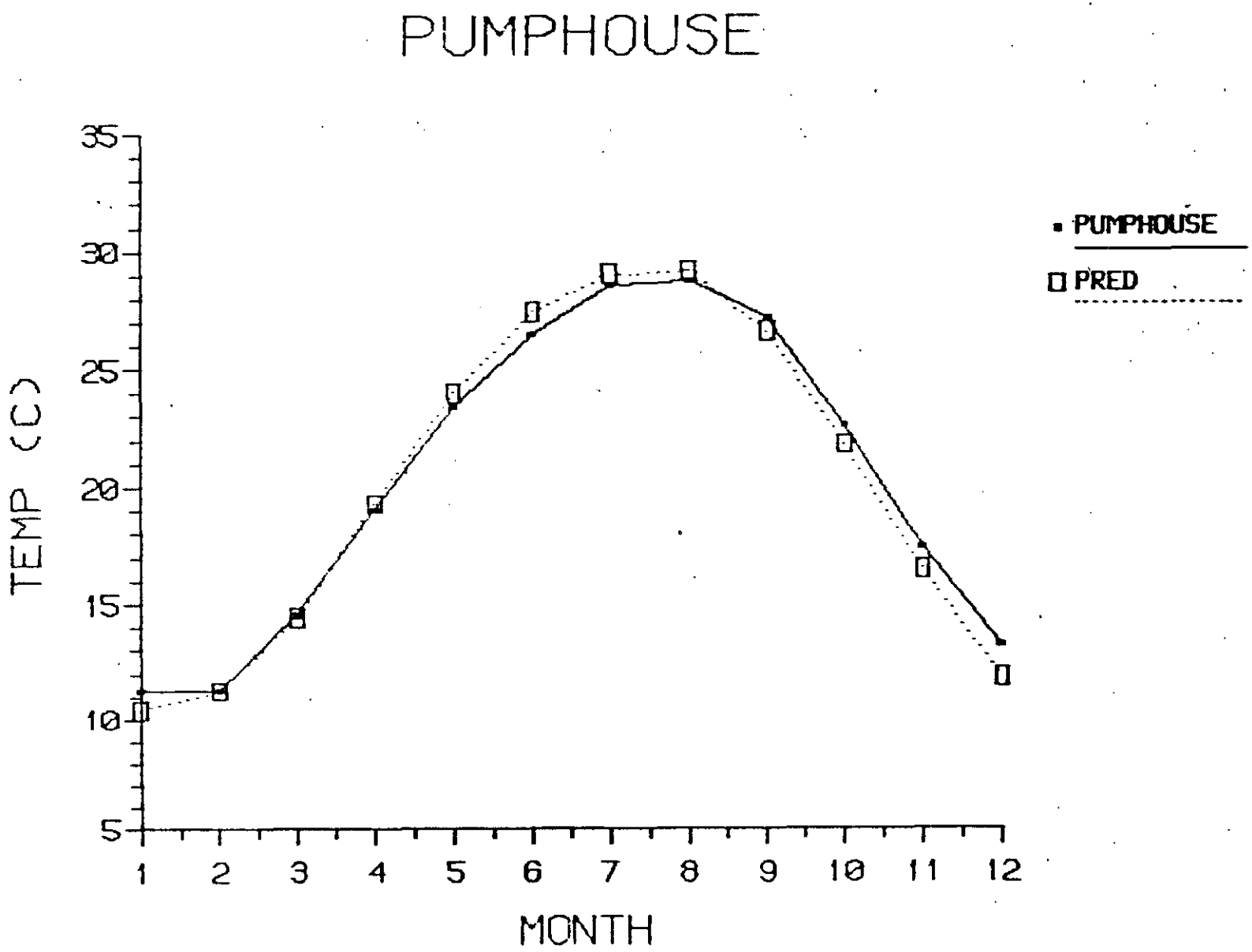

Figure 9. Predicted (PRED) and observed (PUMPHOUSE) monthly mean temperatures for the Par Pond Pumphouse.

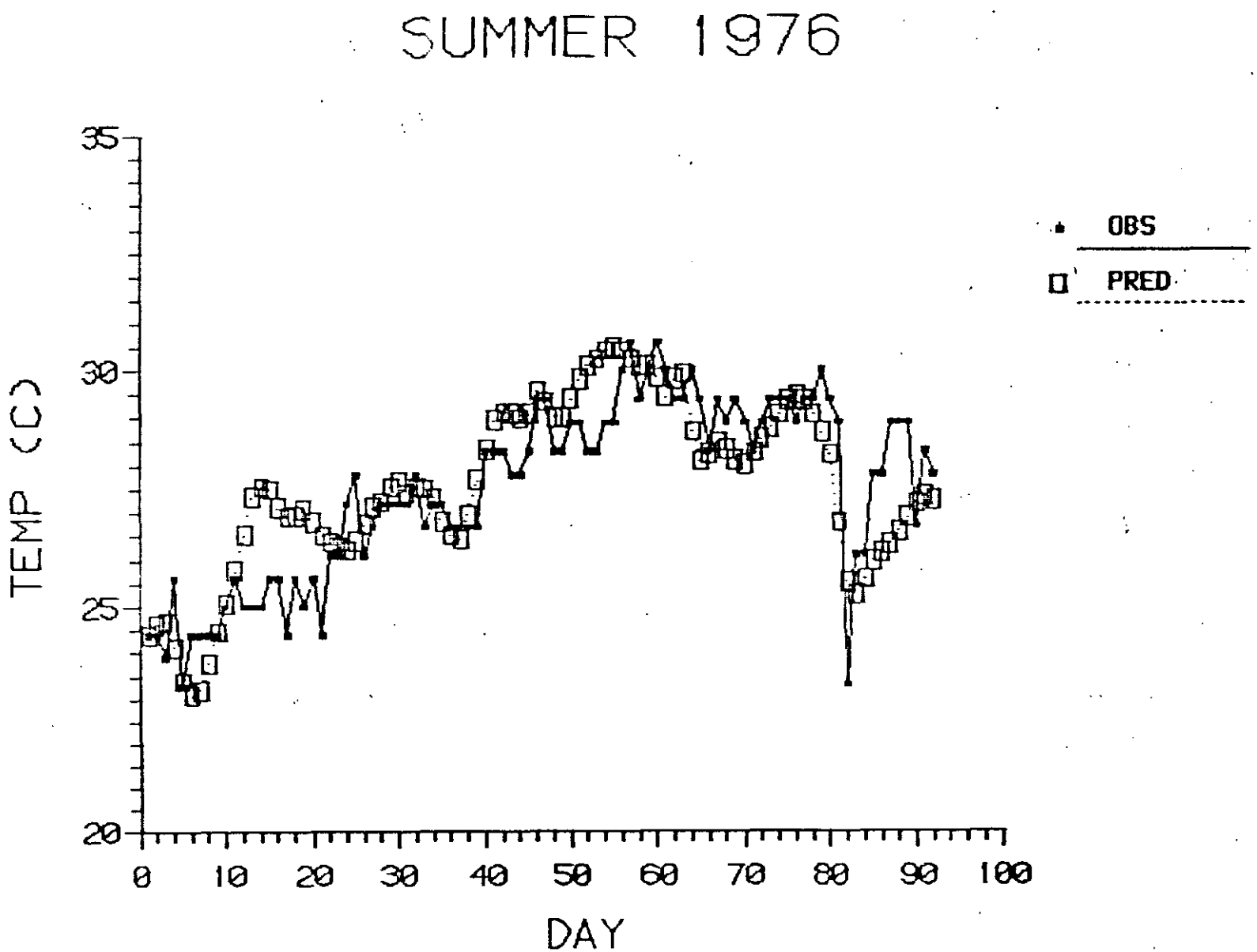

Figure 10. Predicted (PRED) and observed (OBS) daily average surface temperatures for June, July and August 1976 at the Par Pond Pumphouse.

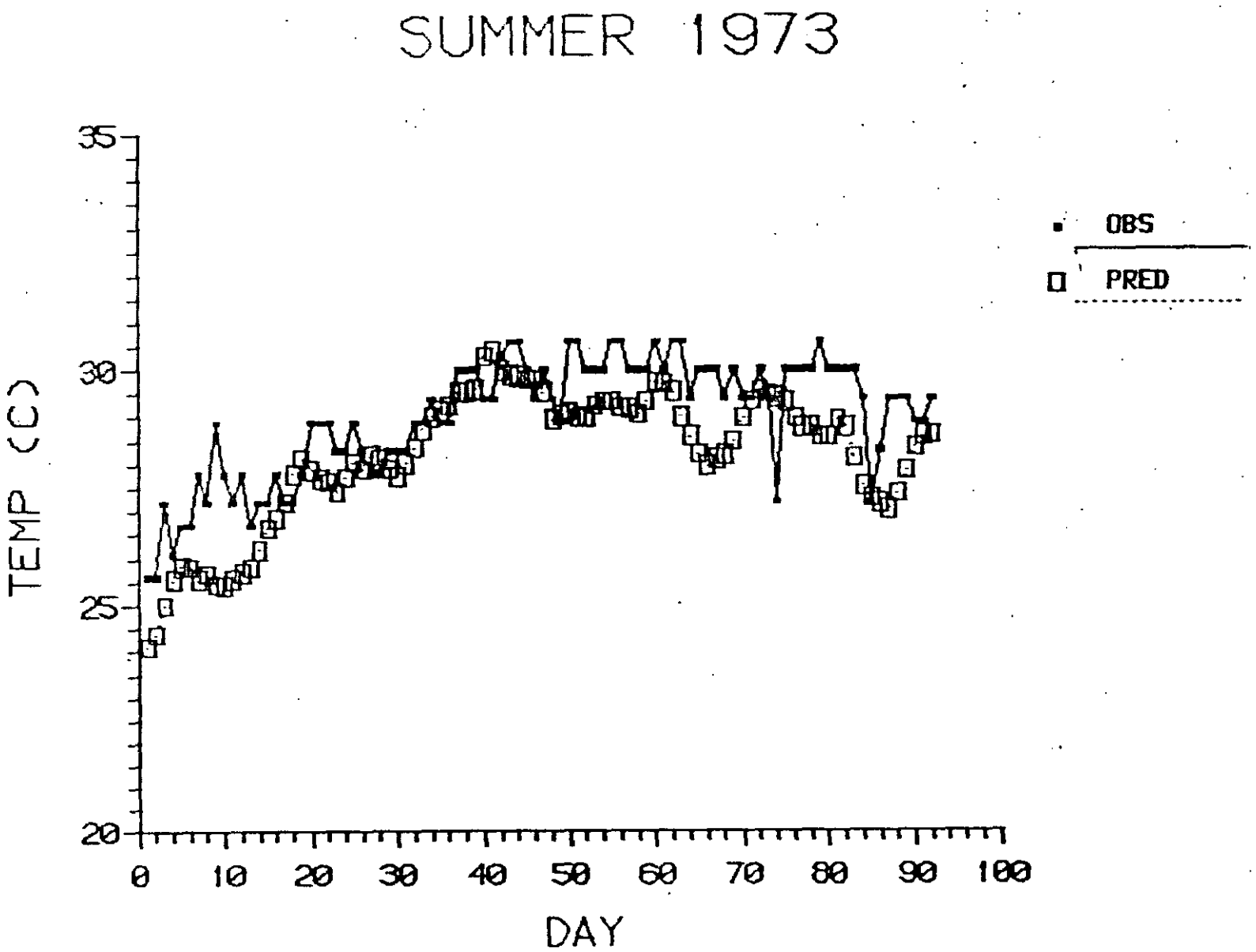

Figure 11. Predicted (PRED) and observed (OBS) daily average surface temperatures for June, July, and August 1973 at the Par Pond Pumphouse.

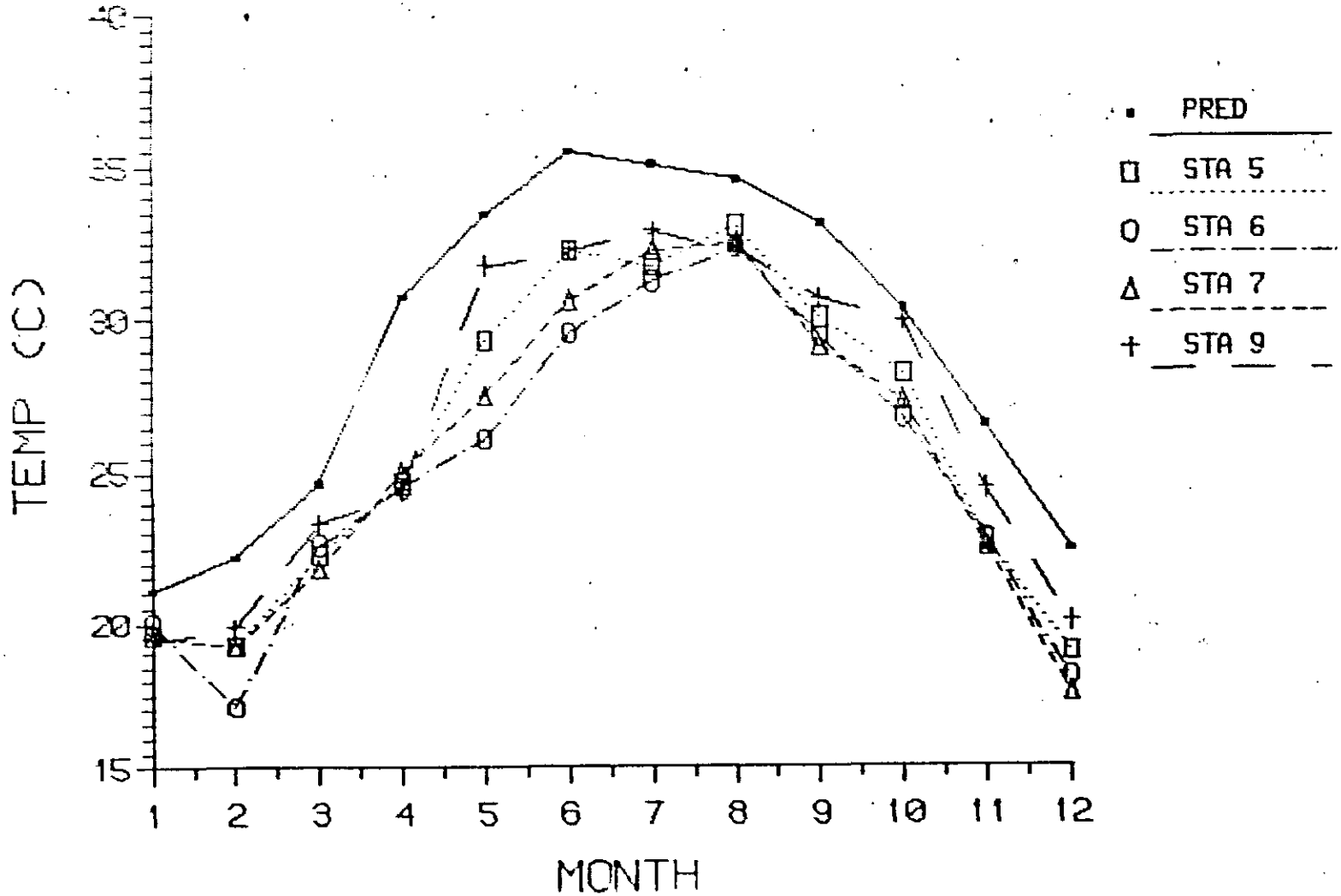

Figure 12. Predicted absolute maximum temperatures for the lower end of the proposed L Area Lake and observed maximum surface temperatures at 4 Par Pond stations relatively unaffected by P Reactor heated water.